Biomacromolecules

Article

Cite This: Biomacromolecules XXXX, XXX, XXX−XXX

pubs.acs.org/Biomac

Marcromolecular Architecture and Encapsulation of the Anticancer Drug Everolimus Control the Self-Assembly of Amphiphilic Polypeptide-Containing Hybrids

Anastasis Karatzas,[†,‡] Johannes S. Haataja,[†,§] Dimitrios Skoulas,[‡] Panayiotis Bilalis,[‡] Spyridon Varlas,[‡] Panagiota Apostolidi,[‡] Sosanna Sofianopoulou,[∥] Efstratios Stratikos,[⊥] Nikolay Houbenov,[§] Olli Ikkala,[§] and Hermis Iatrou*[,‡]

[‡]University of Athens, Department of Chemistry, Panepistimiopolis, Zografou, 15771, Athens, Greece

[§]Aalto University, Department of Applied Physics, FI-00076, Aalto, Espoo, Finland

[∥]Hellenic Republic, Ministry of Rural Development and Food, Athens, Greece

[⊥]National Centre for Scientific Research Demokritos, Patriarhou Gregoriou and Neapoleos 27, Agia Paraskevi 15341, Athens, Greece

Supporting Information

ABSTRACT: Macromolecular architecture plays an important role in the self-assembly process of block copolymer amphiphiles. Herein, two series of stimuli-responsive amphiphilic 3-miktoarm star hybrid terpolypeptides and their corresponding linear analogues were synthesized exhibiting the same overall composition and molecular weight but different macromolecular architecture. The macromolecular architecture was found to be a key parameter in defining the morphology of the nanostructures formed in aqueous solutions as well as to alter the self-assembly behavior of the polymers independently of their composition. In addition, it was found that the assemblies prepared from the star-shaped polymers showed superior tolerance against enzymatic degradation due to the increased corona block density on the outer surface of the nanoparticles. Encapsulation of the hydrophobic anticancer drug Everolimus resulted in the formation of intriguing non-spherical and non-symmetric pH-responsive nanostructures, such as "stomatocytes" and "multi-compartmentalized suprapolymersomes", while the pH-triggered release of the drug was also investigated. Owing to the similarities of the developed "stomatocytes" with red blood cells, in combination with their pH-responsiveness and superior stability over enzymatic degradation, they are expected to present advanced drug delivery properties and have the ability to bypass several extra- and intracellular barriers to reach and effectively treat cancer cells.

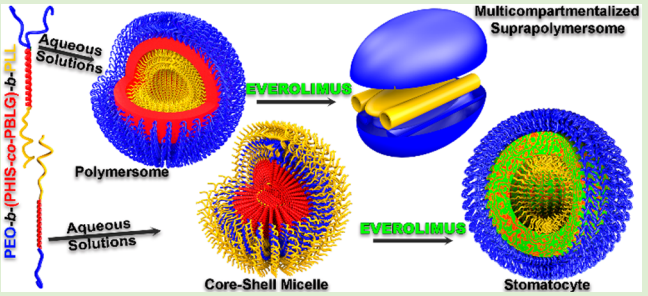

1. INTRODUCTION

In spite of considerable efforts from researchers and clinicians, effective cancer treatment remains an ongoing challenge, while cancer-related mortality increases every year. Conventional chemotherapy still cannot direct the delivery of drugs to cancer cells in a targeted mode and presents significant drawbacks, such as poor aqueous solubility of the existing chemotherapeutics, non-specific biodistribution, severe toxicity to normal cells, inadequate drug concentrations at cancerous cells, and development of multidrug resistance. Recently, nanotechnology has been utilized in order to improve the pharmacokinetics of anticancer drugs.[1−3] Nanoparticles (NPs) self-assembled from amphiphilic block copolymers have demonstrated that they can improve the efficacy as well as the targetability of drugs to tumor cells in both a passive and an active targeting manner. Due to the natural mechanisms of organisms to resist and destroy anything foreign invading their body, there are several extra- and intracellular barriers that hinder the efficacy of the nanocarriers through the blood compartment.[4] Most of the studies thus far have been focused on the control of the functionality (e.g., pH-, temperature-, redox-responsiveness),[5−8] the size and surface chemistry,[9] and the mechanical properties[10] of spherical nanoparticles to improve the biodistribution and effectiveness of NPs, mainly related to bypassing intracellular barriers. Toward this aim, several functionalities have been incorporated in nanocarriers, such as stimuli-responsiveness directed by the unique characteristics of the tumor microenvironment over the healthy cells, as well the attachment of targeting moieties[9] that are overexpressed at the membrane of certain types of

Received: September 27, 2019
Revised: November 5, 2019
Published: November 7, 2019

Downloaded via Efstratios Stratikos on November 19, 2019 at 19:52:38 (UTC).
See https://pubs.acs.org/sharingguidelines for options on how to legitimately share published articles.

© XXXX American Chemical Society

DOI: 10.1021/acs.biomac.9b01331
Biomacromolecules XXXX, XXX, XXX−XXX

cancer cells. It has been found that, in addition to the above characteristics, the shape of the NPs[11,12] (i.e., nanoworms,[13,14] filomicelles,[15,16] nanorods,[17−19] and nanodisks[20,21]) can affect the hemorheological dynamics, cellular uptake capability, tumor targeting, and in vivo biodistribution of the systems. It is evident that, in order to introduce all these functionalities in the same nanocarrier, the complete control of the self-assembly down to the lowest length-scales is required. This has not been achieved up to date, and hence, efficacious patient responses toward nanoparticulate drug delivery remain modest, as shown in a recent study of Wilhelm et al., who reported that only 0.7% (median) of the administered nanoparticle dose is found to be delivered to a solid tumor.[22−24] We believe that the control of these parameters requires the use of multi-functional polymeric materials combined with a complex macromolecular architecture.

Over recent years, polypeptide-containing amphiphilic polymers have become one of the most promising multi-functional platform for the design of drug delivery systems (DDS) compared to conventional synthetic polymers owing to their unique 3D structure that allows for the control of their self-assembly down to the lowest possible length scales, as well as for their enhanced biocompatibility. Branched amphiphilic polymers such as dendrimers and miktoarm stars have been shown to provide superior protection of the NPs and, therefore, longer circulation within the blood compartment, with the obvious advantage of potential improved accumulation to the targeted pathological sites.[25−28] Miktoarm star polymers, presented in the early 1990s by our group,[29,30] were originally synthesized aiming toward the combination of different polymeric materials with completely different properties within the same molecule. It was found that miktoarm stars can control the microphase morphology and volume fraction separately in bulk and influence significantly the aggregation in solution.[31−34]

To date, there is a limited number of publications on the synthesis of miktoarm stars containing polypeptides, since methodologies for the controlled polymerization of α-amino acids have only been recently developed.[35−40] Herein, two series of novel multi-functional amphiphilic linear and 3-miktoarm star hybrid polypeptides were synthesized via ring-opening polymerization (ROP) of the corresponding α-amino acid *N*-carboxy anhydrides (NCAs). In particular, the linear triblock terpolymer analogues were of the ABC type, whereas the miktoarm star-shaped analogues were of the $(A)_2BC$ type, where A is poly(ethylene oxide) (PEO), B is poly(L-histidine-*co*-γ-benzyl-L-glutamate) (P(His-*co*-BLG)), and C is poly(L-lysine hydrochloride) (PLL) (Scheme 1). The polymers were designed in pairs, one linear and its corresponding 3-miktoarm star counterpart, where the polymers in each pair had the same total molecular weight and the same overall composition, but different macromolecular architecture. The molecular weight of the PEO block in all linear polymers was 9.95×10^3 g mol^{-1}, whereas a two-arm PEO macroinitiator of molecular weight for each arm equal to 5.0×10^3 g mol^{-1} was used for the synthesis of the 3-miktoarm star-shaped polymers. The B block was maintained the same in all cases, while the molecular weight of the PLL block was varied. The self-assembly of the synthesized polymers in aqueous media was investigated, and the effect of the macromolecular architecture on the morphology of the formed NPs was also studied. Subsequently, the resistance of the obtained linear and star polymer-based NPs toward enzymatic degradation was monitored upon incubation of the assemblies with proteolytic enzymes.

Scheme 1. Linear (a) and 3-Miktoarm Star (b) Hybrid Polypeptides Synthesized Herein

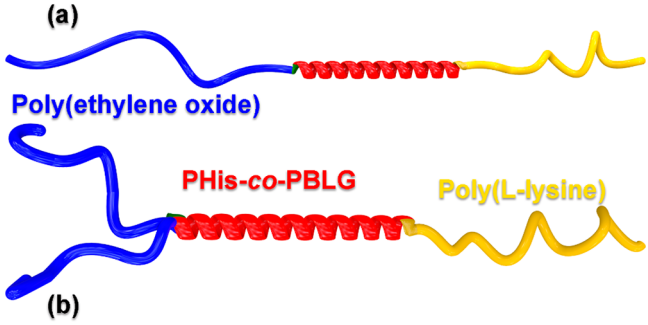

Importantly, the anticancer drug Everolimus was encapsulated into the nanostructures, and the morphology of the drug-loaded assemblies was evaluated, revealing the formation of unique morphologies, including "stomatocytes" and "multi-compartment suprapolymeromes". Finally, the pH-responsive character of both not-loaded and drug-loaded NPs was also investigated and indicated the potential of our systems for on-demand pH-regulated drug release applications.

2. EXPERIMENTAL SECTION

2.1. Materials. BOC-His(Trt)-OH (>99%) was purchased from Christof Senn Laboratories AG. Triphosgene (99%) was purchased from Acros Organics. Thionyl chloride (>99%), L-lysine (>99%), and L-glutamic acid γ-benzyl ester were purchased from Sigma-Aldrich. Triethylamine (>99%, Et_3N, Acros Organics) was dried over calcium hydride for 1 day and then distilled and stored in vacuo over sodium. The appropriate quantity needed was freshly distilled prior to use. Purification of tetrahydrofuran (THF, max 0.005% water, Merck Millipore) was performed over Na−K alloy, using standard high vacuum techniques reported elsewhere.[41] Ethyl acetate (>99.5%, Merck Millipore) was fractionally distilled over phosphorus pentoxide. Hexane (>99%, Merck Millipore) was fractionally distilled over sodium, followed by distillation over *n*-BuLi. Dichloromethane (99.5%) was purchased from Merck Millipore. *N*,*N*-Dimethylformamide (DMF; 99.9+%, Merck Millipore, special grade for peptide synthesis with less than 50 ppm of active impurities) was purified by short-path fractional distillation under high vacuum in a custom-made apparatus, and the middle fraction was used. Benzene (99%, thiophen-free grade, Sigma-Aldrich) was treated with calcium hydride and was allowed to be stirred overnight for moisture removal. It was then distilled under high vacuum and stored in a different flask containing *n*-BuLi. Diethyl ether (99.5+%) was purchased from Sigma-Aldrich. Trifluoroacetic acid (TFA; >99%) was obtained from Merck Millipore. Fluorescamine and trypsin were purchased from Sigma-Aldrich. Poly(ethylene oxide) monomethyl ether (mPEO-OH) with average M_n = 9.95 and 5.0×10^3 g mol^{-1} was purchased from Sigma-Aldrich and was converted to the corresponding amine-functionalized mPEO-NH_2 and $(mPEO)_2$-NH_2 macroinitiators. Leucine aminopeptidase (LAP), 2-(*N*-morpholino) ethanesulfonic acid (MES; 98%), Tris base (99%), OxymaPure (99%), and *N*,*N*′-dicyclohexylcarbodiimide (DCC; 98%) were purchased from Sigma-Aldrich. BOC-Glu-OH (99%) was purchased from Bachem.

2.2. Methods. *2.2.1. NMR Spectroscopy.* ^{1}H NMR spectroscopy was performed using a Bruker400 spectrometer (400 MHz). The spectra of the polymers were obtained in either D_2O + DCl + DMSO-d_6, while the spectra of the NCAs were obtained in $CDCl_3$, at room temperature.

2.2.2. FT-IR Spectroscopy. Fourier Transform-Infrared (FT-IR) spectroscopy measurements were performed using a PerkinElmer

DOI: 10.1021/acs.biomac.9b01331
Biomacromolecules XXXX, XXX, XXX−XXX

Spectrum One instrument, in KBr pellets at room temperature, in the 450−4000 cm^{-1} range.

2.2.3. Size Exclusion Chromatography. Size exclusion chromatography (SEC) was used to determine the M_n and $Đ_M = M_w/M_n$ values. The analysis was performed using two SEC sets. The one was composed of a Waters Breeze instrument equipped with a 2410 differential refractometer and a Precision PD 2020 two-angle (15°, 90°) light scattering detector. The carrier solvent was a 0.10% TFA (v/v) solution of water/acetonitrile (60/40 v/v) at a flow rate of 0.8 mL min^{-1} at 35 °C. Three linear Waters hydrogel columns were used as a stationary phase. For protected polymers, the analysis was performed using a second SEC instrumentation. The system was composed of a Waters 600 high-performance liquid chromatographic pump, Waters Ultrastyragel columns (HT-2, HT-4, HT-5E, and HT-6E), a Waters 410 differential refractometer and a Precision PD 2020 two angles (15°, 90°) light scattering detector at 60 °C. A 0.1 M LiBr in DMF solution was used as an eluent at a rate of 1 mL min^{-1}.

2.2.4. UV Spectroscopy. UV spectroscopy was performed using a PerkinElmer Lamda 650 spectrometer, from 200−500 nm, at room temperature with cells requiring 120 μL. A Waters Diode-Array 690 detector was used for the calibration and online determination of Everolimus drug loading efficiency at λ = 279.4 nm.

2.2.5. Size Measurements. Dynamic light scattering (DLS) measurements were conducted with a Brookhaven Instruments Nanobrook Omni system operating at λ = 640 nm and with 40 mW power. Correlation functions were analyzed by the cumulant method and the Contin software. The correlation function was collected at 90°. All measurements were performed in either an isotonic Tris buffer (10 mM, 150 mM NaCl) at pH = 7.4, MES buffer (10 mM, 150 mM NaCl) at pH = 6.5, or an isotonic acetate buffer (10 mM, 150 mM NaCl) at pH = 5.0. The concentration range measured was between 2×10^{-3} and 1×10^{-5} g mL^{-1}. Static light scattering (SLS) measurements were carried out on an ALV/CGS-3 Compact Goniometer System (ALV GmbH, Langen, Germany), equipped with an ALV-5000/EPP multitau digital correlator with 288 channels and an ALV/LSE-5003 light scattering electronics unit for stepper motor drive and limit switch control. A JDS Uniphase 22 mW He−Ne laser was used as the light source. The instrument was connected to a Polyscience model 9102 bath for temperature control, allowing measurements at variable temperature.

2.2.6. Electrophoretic Mobility. The electrophoretic mobility measurements of the empty and drug-loaded nanoparticle dispersions were conducted using a Brookhaven Instruments Nanobrook Omni system operating at λ = 640 nm and with 40 mW power, operating in PALLS mode. All the measurements were performed in isotonic Tris buffer (10 mM, 150 mM NaCl) at pH = 7.4 at 37 °C and were the average of at least three runs.

2.2.7. Fluorescence Measurements. All fluorescence measurements were performed using a TECAN SPARK 10 M multimode microplate reader using 96-well black microplates (Greiner). To measure the enzymatic degradation of the hybrid terpolypeptide NPs by leucine aminopeptidase (LAP), 30.77 μL of a 48.5 mg mL^{-1} polymer solution in PBS (either linear or star polymer) were mixed with 10 μL of 100 nM LAP in PBS at pH = 7.4. Respectively, for the studies with trypsin, 500 μL of a 3 mg mL^{-1} polymer solution in PBS (either linear or star polymer) were mixed with 4.8 μL of 0.1 nM trypsin in PBS at pH = 7.4. The total volume of the samples tested with LAP was 100 μL and that of the samples tested with trypsin was 2 mL. All the samples were incubated at 37 °C for 0 h, 1 h in the case of trypsin or 24 h in the case of LAP. At the end of the incubation, 10 μL from each sample was mixed with 90 μL of a 1 mg mL^{-1} fluorescamine solution in acetonitrile, 15 μL of 0.1 M borate buffer at pH = 8.0 and 145 μL Milli-Q water. After 5 min, the fluorescence was measured using excitation at λ = 405 nm and emission at λ = 485 nm. PBS samples, LAP samples in PBS (100 nM) or trypsin samples in PBS (0.1 nM), and polymer samples (either linear or star polymer from the stock samples) were also tested as controls. All the experiments were performed in triplicate.

2.2.8. Cryogenic Transmission Electron Microscopy. Cryogenic Transmission Electron Microscopy (Cryo-TEM) imaging was carried out using a JEOL JEM 3200FSC field emission microscope operated at 300 kV in bright field mode with an Omega-type Zero-loss energy filter. The images were acquired using an Ultrascan 4000CCD camera (Gatan) and Gatan Digital Micrograph software, while the specimen temperature was constantly maintained at −187 °C. Vitrified samples were prepared using an FEI Vitrobot by placing 3−4 μL of sample solution on holey carbon grids under 5 and 100% humidity, blotted with filter paper about 0.5−1.5 s for aqueous samples, respectively, and immediately plunged into an ethane/propane mixture at −170 °C and cryo-transferred to the microscope.

2.2.9. Electron Tomography. Electron tomographic tilt series were acquired with the SerialEm-software3 package.[42] Samples were tilted between ±69° angles with 2−3° increments step depending on the beam sensitivity of the sample. Alignment of tilt image series was carried out using Imod software package.[43] Initially, maximum entropy (MEM) reconstruction scheme was implemented using MEM software on a Linux cluster with regularization parameter δ value 5.0×10^{-2}.[44] A total variation (TV) reconstruction scheme was subsequently implemented for improved resolution according to Jensen et al.,[45] and Astra toolbox[46,47] was used for construction of the projection and back projection operators. For isosurface rendering, reconstructed volumes were segmented using trainable Weka segmentation.[48]

2.3. Polymer Synthesis. *2.3.1. Synthesis of Linear mPEO-NH_2 Macroinitiator.* Commercially available poly(ethylene oxide) monomethyl ether (mPEO-OH) with average $M_n = 5.0 \times 10^3$ or 9.95×10^3 g mol^{-1} was converted to its amino-functionalized analogue (mPEO-NH_2) via a two-step procedure.[49] In a typical experiment, mPEO-OH (10 g, average $M_n = 5.0 \times 10^3$ g mol^{-1}, ∼2 mmol) was first dissolved in 60 mL of dichloromethane in a round-bottom flask. Under an argon atmosphere, a 10-fold excess of *p*-toluenesulfonyl chloride (*p*-TsCl, 3.8 g, 20 mmol) and triethylamine (2.8 mL, 20 mmol) was added, and the reaction mixture was stirred at reflux temperature overnight. Then, the polymer was precipitated in excess diethyl ether and filtered. The dissolution (dichloromethane)−precipitation (diethyl ether) procedure was repeated three times in order to remove the excess *p*-TsCl. Finally, the resulting mPEO tosylate was exhaustively dried under high vacuum. In the second step, the dry mPEO tosylate was dissolved in aqueous NH_3 solution 25% (∼60 mL) in a round-bottom flask, and the mixture was vigorously stirred at room temperature for 10 days. After this period, the solution was concentrated in vacuo, and the residue was dissolved in 1 M NaOH solution (∼50 mL). The aqueous solution was stirred for 1 h and then was extracted with dichloromethane (3 × 60 mL). The combined organic phases were concentrated and dried over anhydrous magnesium sulfate. The drying agent was removed by filtration, and the filtrate was poured into excess diethyl ether. The precipitated amino-functionalized mPEO-NH_2 was collected by filtration and dried under vacuum (9.5 g, 1.9 mmol). The synthetic procedure followed is shown in Scheme 2.

2.3.2. Synthesis of Two-Armed $(mPEO)_2$-NH_2 Macroinitiator. The approach followed for the synthesis of the two-armed $(mPEO)_2$-NH_2 macroinitiator involved the reaction of the amino-functionalized mPEO-NH_2 (5.0×10^3 g mol^{-1}) with BOC-protected L-glutamic acid, followed by deprotection of the amine group. In particular, BOC-Glu-OH (0.371 g, 3 mmol −COOH), OxymaPure (0.94 g, 6.6 mmol) and

Scheme 2. Synthetic Procedure of the Amino-Functionalized mPEO-NH_2 Macromolecular Initiator for the Ring-Opening Polymerization of NCAs

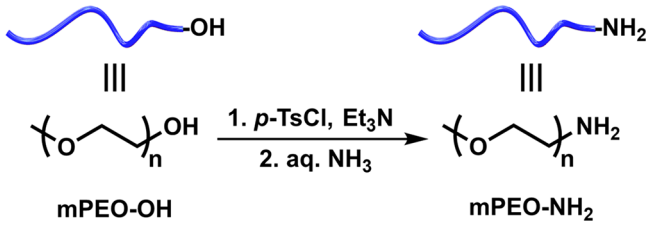

DOI: 10.1021/acs.biomac.9b01331
Biomacromolecules XXXX, XXX, XXX−XXX

Scheme 3. Synthetic Procedure of the Amino-Functionalized Two-Armed $(mPEO)_2$-NH_2 Macromolecular Initiator for the Ring-Opening Polymerization of NCAs

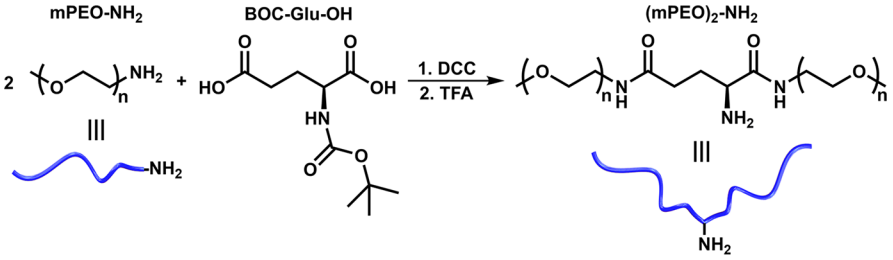

DCC (1.36 g, 6.6 mmol) were dissolved in anhydrous *N*,*N*-dimethylformamide (10 mL). This solution was added to a stirred solution of mPEO-NH_2 (12 g, 2.4 mmol) in 70 mL of anhydrous *N*,*N*-dimethylformamide. The reaction mixture was stirred in a sealed round-bottom flask at room temperature overnight. The following day, an additional amount of OxymaPure (0.47 g, 3.3 mmol) and DCC (0.68 g, 3.3 mmol) dissolved in anhydrous *N*,*N*-dimethylformamide (5 mL) was added and stirring was continued overnight. The cloudy solution was diluted with dichloromethane (50 mL) and filtered through Celite. The clear filtrate was concentrated until dryness, and the residue was dissolved in dichloromethane (60 mL). The solution was poured into excess diethyl ether (500 mL), and the precipitated solid was obtained by filtration and dried in a vacuum oven.

The coupling step was followed by the purification step, that is, the separation of $(mPEO)_2$-NH(BOC) macroinitiator from the mPEO-NH_2 precursor. Initially, the mixture of the two polymers was subjected to fractional precipitation and after the deprotection procedure, dialysis was utilized for removal of the remaining unreacted amino-functionalized mPEO-NH_2. The solid obtained from the first step was dissolved in chloroform so that a 5−10% w/v concentration was achieved. In particular, 12 g of the crude solid product were dissolved in 200 mL of chloroform at room temperature. The solution was placed to a separatory funnel, and *n*-heptane was added portionwise (per 100 mL) under transient shaking until a permanently turbid solution was achieved. In general, twice the amount of *n*-heptane was required in order to obtain the aforementioned turbid solution (500 mL). The resulting solution was then gently heated using a heat gun with simultaneous shaking, and the obtained clear solution was left to stand at ambient temperature. After a period of time, ranging from 3 h to overnight, two phases were distinguishable in the separatory funnel. The upper phase was transparent with low viscosity and the lower phase was viscous and translucent. The latter one, which mainly contained the polymer with higher molecular weight, was collected. An additional amount of *n*-heptane (100 mL) was added and the above-described procedure of heating and standing was repeated. Another translucent fraction was collected. In total, three viscous fractions were collected. The fourth one mainly consisted of mPEO-NH_2 precursor was decanted. The whole procedure was monitored by size exclusion chromatography. The combined fractions were concentrated, and the residue was dissolved in dichloromethane and then precipitated in excess diethyl ether. After drying, 8 g of white solid were isolated and were dissolved in 30 mL of dichloromethane. To the solution, 30 mL of trifluoroacetic acid was added and the obtained solution was stirred for 1.5 h at room temperature for quantitative removal of the BOC protecting group. At this time, the solution was concentrated, and the solid residue was dissolved in 30 mL of Milli-Q water containing 10 g of NaCl. The pH was adjusted to 12 with 1 M aqueous NaOH solution and the mixture was stirred at room temperature for 30 min. The aqueous solution was extracted with dichloromethane (2 × 100 mL), and the combined organic phases were directly poured into excess diethyl ether. The precipitated solid was filtered and dried under vacuum.

The last step of $(mPEO)_2$-NH_2 macroinitiator preparation involved dialysis (MWCO 6−8 kDa) for removal of the remaining proportion of unreacted mPEO-NH_2 and other low molecular weight substances. In general, the aqueous polymer solution has to be diluted enough and contact time with the external solvent (Milli-Q water) has to be minimized for completion of the separation without the loss of desired two-armed macroinitiator. The whole procedure was monitored by size exclusion chromatography. Finally, excess amount of water was removed by distillation using high vacuum techniques, and final fractions of water were sublimated by lyophilization procedure. The pure $(mPEO)_2$-NH_2 macroinitiator (∼3 g) was stored at −20 °C. The synthetic procedure followed is shown in Scheme 3.

2.3.3. Synthesis of the Linear and Star Polymers. All polymers were synthesized by ring-opening polymerization (ROP) using high vacuum techniques according to the general synthetic procedure described below.[41,50] Each polymerization was performed in a custom-made apparatus. The synthetic pathway followed for the synthesis of the miktoarm stars are given in Scheme 4. A similar procedure was utilized for the synthesis of linear polymers. Details for the polymerization procedure are given in the SI.

2.4. Self-Assembly of Empty NPs via Solvent-Switch. The self-assembly behavior of NPs was studied at three different isotonic buffers with different pH values, that is, pH = 7.4, 6.5, and 5.0. For that purpose, three different buffers were prepared, each at 10 mM concentration containing 150 mM NaCl. A Tris buffer was used at pH = 7.4 and was prepared by dissolving the appropriate amount of solid Tris in Milli-Q water, followed by addition of the appropriate amount of NaCl and concentrated aqueous solution of HCl for pH adjustment. A MES buffer was used at pH = 6.5 and was prepared by dissolving the appropriate amount of 2-(*N*-morpholino) ethanesulfonic acid and NaCl in Milli-Q water, followed by titration with an aqueous solution of 10 M NaOH for pH adjustment.

Finally, an acetate buffer was used at pH = 5.0 and was prepared by dissolving an appropriate amount of glacial acetic acid and NaCl in Milli-Q water followed by titration with an aqueous solution of 10 M NaOH for pH adjustment. In a typical experiment, 10 mg of the hybrid terpolypeptides were dissolved in 4 mL of DMSO. After complete dissolution, 4 mL of each buffer were slowly added dropwise within 30 min and were left for 1 h under vigorous stirring. The solution was then placed in a dialysis bag (Spectrapor MWCO 3500, 30 °C) and was dialyzed against 2 L of appropriate isotonic buffer for 4 h. The dialysis was repeated another three times with 2 L of buffer, one for 4 h, the second overnight for 12 h, and the third for another 4 h, for complete removal of DMSO.

2.5. Loading of Anticancer Drug Everolimus. Everolimus is a rather hydrophobic drug with a high molecular weight of 958 g mol^{-1}. The above described solvent-switch methodology was utilized for drug encapsulation. Several drug/polymer weight ratios were used in order to obtain the optimum values with the highest Everolimus encapsulation efficiency. When the ratio was high, that is, greater than 0.3, it was found that excess non-encapsulated drug was present that precipitated, while the amount of encapsulated drug remained stable for the same weight of polymer. Therefore, in order to obtain the optimum encapsulation efficiency, an Everolimus/polymer weight ratio of 0.3 was chosen. In a typical experiment, 10 mg of the hybrid terpolypeptides were dissolved in 4 mL of DMSO. After complete dissolution, 3 mg of Everolimus were added in the polymer solution

DOI: 10.1021/acs.biomac.9b01331
Biomacromolecules XXXX, XXX, XXX−XXX

Scheme 4. Synthetic Pathway Followed for the Preparation of (A) the Linear mPEO-*b*-P(His-*co*-BLG)-*b*-PLL Triblock Quarterpolymers, and (B) the Branched 3-Miktoarm Star $(mPEO)_2$-*b*-P(His-*co*-BLG)-*b*-PLL Triblock Quarterpolymers

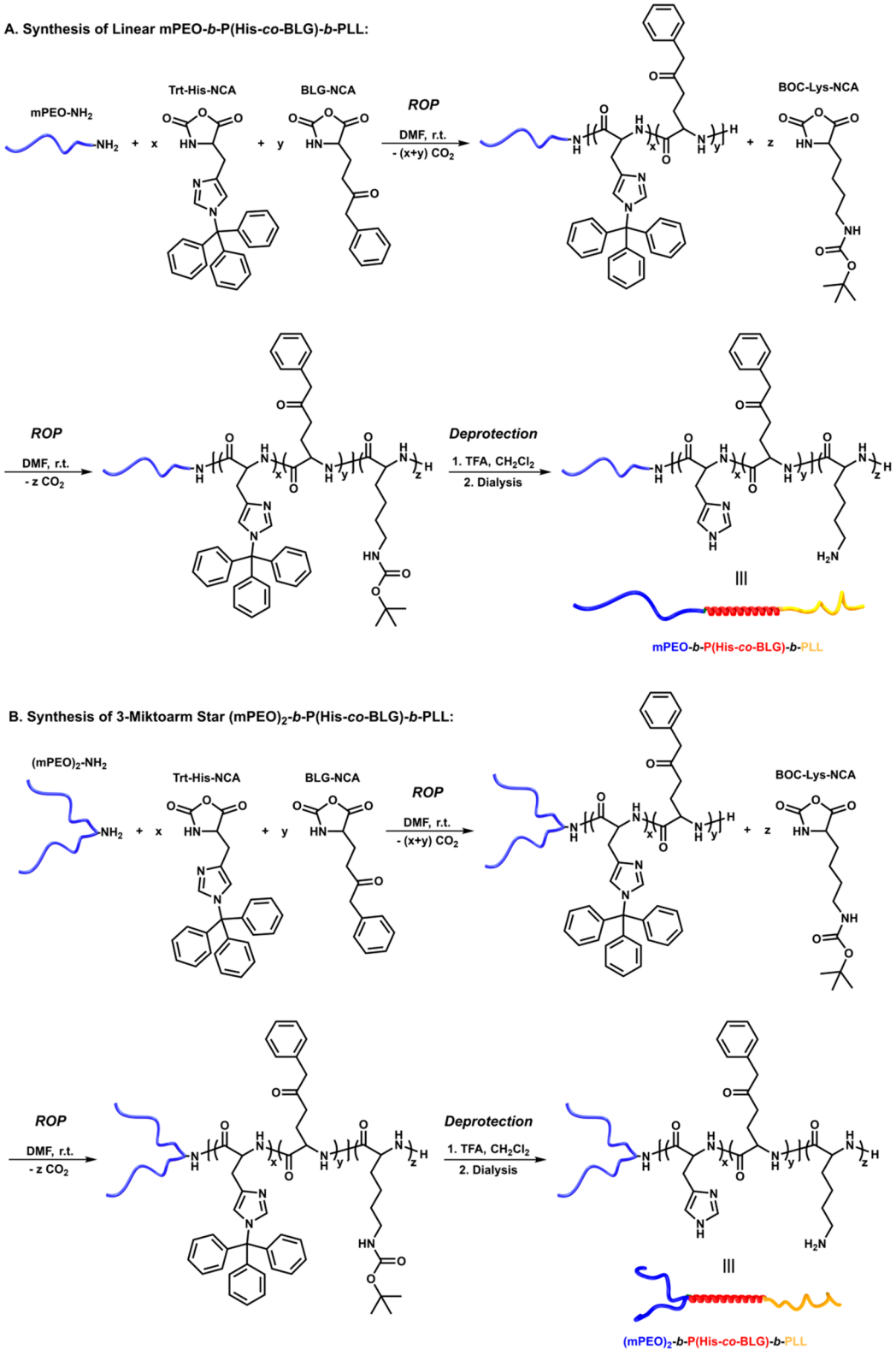

and was stirred for 30 min to allow for its dissolution. Then, 2 mL of buffer was added dropwise to the DMSO solution over a period of 30 min. The solution was then placed in a dialysis bag (Spectrapor MWCO 12−14 kDa, 30 °C) and was dialyzed against isotonic 10 mM Tris buffer at pH = 7.4 (150 mM NaCl, 10 mM Tris), in a volume of 4 L of buffer. After 3 h of dialysis, the dialysis membrane was transferred in fresh isotonic Tris buffer and was dialyzed for an additional period of 3 h again with another 4 L of buffer. The same procedure was repeated one more time, and the NP solution was dialyzed for 12 h. Finally, the volume of the solution was about 12 mL. Then, 2 mL was removed from the solution inside the membrane prior to loading efficiency analysis, while the rest of the solution was

DOI: 10.1021/acs.biomac.9b01331
Biomacromolecules XXXX, XXX, XXX−XXX

split at three equal parts and each part was placed in a new dialysis membrane with the same MWCO and was immediately immersed in 50 mL of buffers at different pH values. In all cases, the clip at the bottom of the dialysis membrane was magnetic, so that the membrane was stirred at 800 rpm during the dialysis procedure.

2.6. Determination of Everolimus Loading in the NPs. The amount of Everolimus loaded in the nanoparticles was determined by SEC analysis using the DMF/LiBr system and an appropriate set of columns focused for retention of low molecular weight species (Styragel HT2) in order to separate the polymer from the drug. Quantification was performed by setting a calibration curve of Everolimus in DMF, where the drug is fully soluble. In a typical experiment, 2 mL of the aqueous NPs solution containing Everolimus in isotonic buffer was extracted with 2 mL of chloroform. The lower organic layer was removed and the extraction was repeated three times. The total amount of chloroform solution containing Everolimus and a small amount of polymer were injected in the SEC system with the DMF/LiBr as the mobile phase and was analyzed using the Diode Array detector at λ = 279.4 nm. The two species were clearly separated and the peak corresponding to Everolimus was quantified using the drug calibration curve. Everolimus loading is given through the loading efficiency (LE; %; mass of Everolimus in NPs/mass of Everolimus in the initial solution) and loading content (LC; %; mass of Everolimus in NPs/mass of polymer). All measurements were carried out in triplicate and the loading results are reported as their average.

2.7. In Vitro Drug Release Studies. In vitro drug release studies were performed at three different pH values (pH = 7.4, 6.5 and 5.0) at 37 °C for pH = 7.4, while 40 °C was applied at pH = 6.5 and 5.0. The original dialysis solution after the drug loading procedure was split in four parts. One part was used to determine the concentration of the drug into the NPs, while the other three were used for in vitro drug release studies at different pH values. The dialysis membrane containing 3 mL of solution of NPs in Tris buffer at pH = 7.4 was immediately immersed in a solution of 50 mL of the corresponding buffer, and the cumulative release of the drug was measured at the exterior solution at defined time intervals. The dialysis membrane was transferred into a fresh buffer solution at every interval, in order to avoid saturation of the solution from the hydrophobic drug. In a typical experiment, 10 mL of the exterior solution were extracted with 2 mL chloroform twice, and 250 μL of the chloroform solution containing Everolimus were subsequently injected in the SEC instrument using DMF/LiBr as the mobile phase featuring the Diode Array detector. The Everolimus concentration was measured by UV spectroscopy at λ = 279.4 nm, using a calibration curve obtained with solutions of known Everolimus concentration measured using the same instrument.

3. RESULTS AND DISCUSSION

3.1. Synthesis of *N*-Carboxy Anhydrides (NCAs). The synthesis of Trt-His-NCA, BLG-NCA, and BOC-Lys-NCA has been discussed in detail in previous publications of our group.[51−53] The high purity of the NCA monomers is crucial for their successful living ring-opening polymerization (ROP) utilizing primary amine functionalized initiators,[50] as confirmed by ^{1}H NMR and FT-IR spectroscopic analysis, discussed previously.[54] BOC-Lys-NCA was chosen as the resulting polymer that can be orthogonally deprotected in the presence of PBLG, since it is well established that the BOC-protecting group can be selectively deprotected using TFA, while the benzyl ester groups of PBLG remain intact.

3.2. Synthesis of the Linear mPEO-NH_2 Macroinitiator. In order to prepare hybrid copolypeptides with high blocking efficiencies via living ROP of the corresponding NCAs, it was critical to synthesize amino end-functionalized poly(ethylene oxide) macroinitiators with high end-group fidelity. After attempting several different synthetic approaches, we identified that the optimal methodology was that reported herein, which resulted in a high degree of transformation of the hydroxyl end-groups to amine groups. However, the size exclusion chromatograms (SEC) of the mPEO derivatives before and after the transformation were nearly identical. The high degree of functionalization was confirmed by synthesizing diblock copolymers for the formation of a polypeptide block, where no trace of the mPEO-NH_2 macroinitiatorwas apparent, indicating that at least 95% of the hydroxyl groups were transformed to amine groups.

3.3. Synthesis of the Two-Armed $(mPEO)_2$-NH_2 Macroinitiator. The synthesis of the two-armed amino-functionalized macroinitiator $(mPEO)_2$-NH_2 and its purification process were monitored by SEC analysis. After dialysis, the excess unreacted linear mPEO-NH_2 was completely removed. The dialysis procedure was monitored by periodically withdrawing aliquots from the dialysis membrane and directly injecting them in the aqueous SEC instrument and was stopped when the linear precursor trace had completely disappeared. The corresponding SEC traces of mPEO-NH_2 macroinitiator and $(mPEO)_2$-NH_2 macroinitiator before and after purification are shown in Figure S1 (see SI). The molecular weight of the single arm precursor was 5.0×10^3 g/mol, while the molecular weight of the 2-arm macroinitiator was exactly 10.0×10^3 g/mol. The polydispersity indices of both, the single arm precursor as well as of the two-armed $(mPEO)_2$-NH_2 macroinitiator were as low as 1.03.

3.4. Synthesis of Linear and 3-Miktoarm Star Hybrid Triblock Terpolypeptides. Two series of hybrid triblock terpolypeptides were synthesized via sequential ROP of the corresponding NCAs using either mPEO-NH_2 or $(mPEO)_2$-NH_2 as the macroinitiator, one linear of the type mPEO-*b*-P(His-*co*-BLG)-*b*-PLL, and one star of the type $(mPEO)_2$-*b*-[P(His-*co*-BLG)-*b*-PLL], where the blocks in the brackets represent each arm of the 3-miktoarm star hybrid terpolypeptide. The synthetic strategy followed for the preparation of the branched polymers is summarized in Scheme 4. A similar strategy was followed for the synthesis of the linear terpolypeptides, with the only difference being the utilization of the monoamino end-functionalized mPEO-NH_2 rather than the two-armed amino-functionalized $(mPEO)_2$-NH_2 macroinitiator. In order to elucidate the influence of the molecular architecture to the self-assembly properties, the polymers were designed as follows: The total molecular weight of the two mPEO arms of the star polymers (M_n = 10.0×10^3 g/mol) was almost equal to the molecular weight of the single mPEO arm (M_n = 9.95×10^3 g/mol) of the linear polymers. The middle block of all hybrid triblock terpolypeptides synthesized herein (linear and star) was a common pH-responsive block comprised of a random copolymer of PHis and PBLG, where PBLG is 18% molar ratio of the total block, with total molecular weight of about 7.0×10^3 g mol^{-1} after deprotection of the PHis units. Finally, in each case the molecular weight of the PLL third block was either 7.0×10^3, 15.0×10^3, 25.0×10^3, or 45.0×10^3 g mol^{-1}. Therefore, for each linear triblock terpolypeptide there exists a corresponding branched one, having the same block composition as well as total molecular weight, but that differs only in its macromolecular architecture (namely, L7-S7, L15-S15, L25-S25, and L45-S45, L for linear and S for stars). A random copolypeptide was chosen as the middle block based on findings from a previous publication of our group, revealing that the incorporation of hydrophobic units in the PHis block can lower the pK_a of the polymer to 6.1

DOI: 10.1021/acs.biomac.9b01331
Biomacromolecules XXXX, XXX, XXX−XXX

Table 1. Molecular Characteristics of the Hybrid Linear Triblock Terpolypeptides of the Type mPEO-*b*-P(His-*co*-BLG)-*b*-PLL[a]

polymer	$M_{n,PEO}$[b] ($\times 10^{-3}$ g mol^{-1})	$M_{n,P(His\text{-}co\text{-}BLG)}$ ($\times 10^{-3}$ g mol^{-1}) Prot.[b]/Deprot.[d]	N_{PHis}/N_{BLG}[c]	$M_{n,PLL}$ ($\times 10^{-3}$ g mol^{-1}) Prot.[b]/Deprot.[d]	$M_{n,Prot.Triblock}$[b] ($\times 10^{-3}$ g mol^{-1})	$M_{n,Deprot.Triblock}$[d] ($\times 10^{-3}$ g mol^{-1})	$Đ_{M,Deprot.}$[d]
L7	9.95	16.0/6.70	38/7	12.5/7.0	38.6	23.7	1.10
L15	9.95	15.6/6.65	37/7	26.4/14.8	52.5	31.4	1.12
L25	9.95	15.9/6.75	38/7	45.6/25.6	71.2	44.0	1.11
L45	9.95	16.6/6.95	40/7	77.8/43.7	106.0	60.6	1.16

[a]Abbreviations: Prot., protected; Deprot., deprotected. [b]Obtained by SEC-TALLS using DMF with 0.1 M LiBr as the eluent at 60 °C. [c]Obtained by ^{1}H NMR spectroscopy in D_2O with a few drops of DCl. [d]Obtained by SEC-TALLS using 0.10% TFA (v/v) solution of H_2O/MeCN (60/40 v/v) as the eluent at 35 °C.

Table 2. Molecular Characteristics of the Hybrid 3-Miktoarm Star Triblock Terpolypeptides of the Type $(mPEO)_2$-*b*-P(His-*co*-BLG)-*b*-PLL[a]

polymer	$M_{n,PEO}$[b] ($\times 10^{-3}$ g mol^{-1})	$M_{n,P(His\text{-}co\text{-}BLG)}$ ($\times 10^{-3}$ g mol^{-1}) Prot.[b]/Deprot.[d]	N_{PHis}/N_{BLG}[c]	$M_{n,PLL}$ ($\times 10^{-3}$ g mol^{-1}) Prot.[b]/Deprot.[d]	$M_{n,Prot.\ Triblock}$[b] ($\times 10^{-3}$ g mol^{-1})	$M_{n,Deprot.\ Triblock}$[d] ($\times 10^{-3}$ g mol^{-1})	$Đ_{M,Deprot.}$[d]
S7	10.0	15.7/6.65	37/7	12.8/7.1	38.3	23.9	1.13
S15	10.0	16.1/6.70	38/7	25.4/14.1	51.1	30.6	1.11
S25	10.0	16.2/6.70	39/7	44.6/24.6	70.3	42.0	1.10
S45	10.0	15.6/7.10	37/8	79.0/44.7	103.9	62.0	1.14

[a]Abbreviations: Prot., protected; Deprot., deprotected. [b]Obtained by SEC-TALLS using DMF with 0.1 M LiBr as the eluent at 60 °C. [c]Obtained by ^{1}H NMR spectroscopy in D_2O with a few drops of DCl. [d]Obtained by SEC-TALLS using 0.10% TFA (v/v) solution of H_2O/MeCN (60/40 v/v) as the eluent at 35 °C.

rather than 6.7, which was previously measured for a PHis homopolymer of the same molecular weight. There are two different pH values that a drug delivery system can respond, the extracellular pH of a cancer tissue which is approximately 6.7−6.8,[55] close to the pK_a value of the PHis homopolymer[54] and the pH of the early endosome, which is lower than 6.5.[56] Therefore, when a pH-responsive drug delivery system is designed to deliver encapsulated anticancer agents inside cancer cells rather than their extracellular vicinity, a pK_a lower than 6.7 should be chosen. In our case, a drug delivery system that targets the intracellular microenvironment was originally designed. Since the only differences between the two series of the prepared polymers regard their macromolecular architecture and the molecular weight of the PLL block, the abbreviation of the linear and star polymers was defined by these characteristics. Therefore, the abbreviation L15 refers to the linear triblock terpolymer with $M_{n,PLL}$ = 15.0 × 10^3 g mol^{-1}, while S15 refers to the 3-miktoarm star with the same PLL molecular weight.

The polymer synthesis was performed using high vacuum techniques.[41] The random distribution of the copolymerized PBLG and PHis units was proved through the increased solubility of the protected diblock copolypeptide in DMF resulting from the copolymerization of Trt-His and BLG NCAs. In case the copolymers were "blocky", the middle P(His-*co*-BLG) block would be insoluble in the polymerization solvent, DMF, whereas all polymerizations conducted in the present study were homogeneous, proving the random distribution of the two monomers across the second bock. The selective deprotection of Trt-His and BOC-Lys monomeric units, by simultaneous quantitative retention of the benzyl protecting groups of L-glutamic acid, was of paramount importance for the functionality of the developed polymers. It is well-known that BOC- and Trt-protecting groups can be orthogonally cleaved under acidic conditions in the presence of the benzyl protecting group of L-glutamic acid.[57,58] The completion of the polymerization kinetics and deprotection processes were monitored by ^{1}H NMR and FT-IR spectroscopy, revealing that 7 days were required for complete monomer consumption during the polymerization of the mixture of Trt-His-NCA with the BLG-NCA, while three days were required for the BOC-Lys-NCA. The final deprotected polymers were exhaustively characterized by size exclusion chromatography featuring a two-angle laser light scattering detector (SEC-TALLS), and ^{1}H NMR and FT-IR spectroscopy. In all cases, molecular weight distributions were monomodal with no apparent traces of low molecular weight species and exhibiting low dispersity values ($Đ_M$ < 1.2; Figure S2, see SI). The ^{1}H NMR spectrum of the branched hybrid terpolypeptide exhibiting 7.0 × 10^{3}g/mol of the PLL block is shown in Figure S3 (see SI). The obtained results for the synthesized linear and 3-miktoarm star triblock terpolymers are summarized in Tables 1 and 2.

3.5. Self-Assembly of the Not-Loaded Hybrid Triblock Terpolypeptides. Nanostructure formation based on the self-assembly of the synthesized amphiphilic linear and 3-miktoarm star hybrid terpolypeptides was achieved by a solvent-switch methodology from the good solvent DMSO into aqueous solutions of appropriately adjusted pH values (i.e., pH = 7.4, 6.5, or 5.0) via dialysis. Self-assembly and nanoparticle (NP) development were driven by the partial insolubility of the middle *a*-helix-forming P(His-*co*-BLG) block in aqueous media. The self-assembly behavior of the deprotected linear and star polymers was studied by DLS, SLS and zeta-potential analysis. It should be mentioned that it was not possible to perform cryo-TEM imaging of the empty NPs, most possibly due to disruption of the nanostructures during the vitrification procedure. Therefore, only indirect results for their structure were obtained through DLS and SLS measurements. Moreover, the stability of the formed NPs toward proteolytic enzymes was monitored through enzymatic degradation studies.

DOI: 10.1021/acs.biomac.9b01331
Biomacromolecules XXXX, XXX, XXX−XXX

Table 3. Summary of Characteristics of the Empty Self-Assembled Nanostructures at Different pH Values at 37 °C

polymer	diameter, D_h[a] (nm; 90°), pH = 7.4	KCounts	diameter, D_h[a] (nm; 90°), pH = 6.5	KCounts	diameter, D_h[a] (nm; 90°), pH = 5.0	KCounts	zeta-potential[b] (mV), pH = 7.4	R_G/R_H,[c] pH = 7.4
L7	76 ± 2	459 ± 15	44 ± 1, 160.4 ± 3	403 ± 13	230.4 ± 4	103 ± 9	+11.5 ± 0.9	0.76
S7	66 ± 1	402 ± 13	79.8 ± 2	381 ± 11	270.5 ± 5	98 ± 7	+18.3 ± 1.1	0.74
L15	64 ± 1	405 ± 14	100.2 ± 2	371 ± 10	560.4 ± 7	92 ± 6	+24.5 ± 1.4	0.75
S15	188 ± 2	550 ± 18	210.5 ± 4	503 ± 15	452.4 ± 6	82 ± 7	+3.8 ± 0.3	1.02
L25	94 ± 2	410 ± 14	103.5 ± 2	371 ± 11	360.4 ± 5	79 ± 9	+35.1 ± 1.6	1.02
S25	89 ± 2	406 ± 13	100.9 ± 2	369 ± 10	310.5 ± 4	74 ± 9	+30.5 ± 1.4	0.98
L45	114 ± 3	410 ± 14	125.4 ± 2	361 ± 11	380.4 ± 4	65 ± 2	+31.8 ± 1.4	1.01
S45	55 ± 1	350 ± 10	65.3 ± 1	321 ± 9	330.5 ± 4	60 ± 14	+31.5 ± 1.5	0.78

[a] D_h values measured from DLS analysis (the error shows the standard deviation from five repeat measurements). [b] Zeta-potential values measured from microelectrophoretic analysis at pH = 7.4. [c] R_G/R_H ratio determined from SLS and DLS analysis.

3.6. Effect of the Macromolecular Architecture on NP Structure. In a previous publication, we had shown that a mPEO-*b*-PBLG-*b*-PLL triblock terpolymer bearing two hydrophilic blocks at the two ends of each chain and a hydrophobic middle block was able to self-assemble into polymersomes, where the hydrophilic chain with the larger volume fraction remained at the outer periphery of the nanostructures.[59] We envisioned that, by altering the macromolecular architecture of the polymer from linear to 3-arm star, keeping the overall molecular characteristics unchanged (i.e., composition and total molecular weight), we would be able to control the shell composition of the NPs formed, independently of the volume fraction of the water-soluble PEO and PLL blocks. Due to the higher density of PEO chains close to the corona−core interface in the case of the star architectures, it would be possible to obtain a polymer nanostructure where the interface must be curved inward to the single P(His-*co*-BLG)-*b*-PLL arm even though the volume fraction of the hydrophilic PLL block would be larger. In the case of the linear hydrophilic chains with the same composition, we hypothesized that the opposite corona preference would occur where, as commonly observed, the hydrophilic part with the larger volume fraction would be located at the outer periphery of the synthesized NPs. Therefore, even for low molecular weight PEO branched chains, the hydrophilic PEO blocks would remain at the outer periphery and form the corona of the NPs, which is preferred in order for the NPs to maintain a "stealth" character toward the immune system. In addition to the effect of the macromolecular architecture, the pH-responsiveness of the NPs was also studied by DLS, SLS as well as electrophoretic mobility measurements. The obtained characterization results of the assemblies resulting from each different polymer composition are shown in Table 3.

An R_G/R_H value close to 0.75 indicates a spherical core−shell micellar structure of the aggregate, while a value close to 1.00 indicates the formation of a bilayer vesicular structure.[60−63] In the case of the vesicular structures, the hydrophilic domains are either located in the outer periphery or in the inner aqueous lumen of the assemblies. Based on the R_G/R_H value of the L7 and S7 polymers (R_G/R_H = 0.76 and 0.74, respectively), light scattering analysis indicates their self-assembly into compact core−shell structures for both polymers. This also indicates that for both polymers the cores of the obtained NPs are comprised of the P(His-*co*-BLG) pH-responsive copolypeptide, with a mixed corona domain composed of both hydrophilic PLL and PEO polymers (Scheme 5b). The zeta potential value of the S7 nanostructures (+18.3 ± 1.1 mV) was more positive than that of the corresponding linear hybrid terpolypeptide L7 (+11.5 ± 0.9 mV). This is expected since, in case of the linear polymer, the positively charged PLL chains are shorter than the PEO blocks (Scheme 6b) and thus the charged units are less exposed at the outer periphery of the NPs than in the case of the star polymer where the PEO chains are shorter as compared to the PLL

Scheme 5. Schematic Representation of the Aggregates Obtained in Aqueous Solutions: (a) Vesicular Structure Obtained from the S15 and (b) Core-Shell Micelle Obtained from the L15[a]

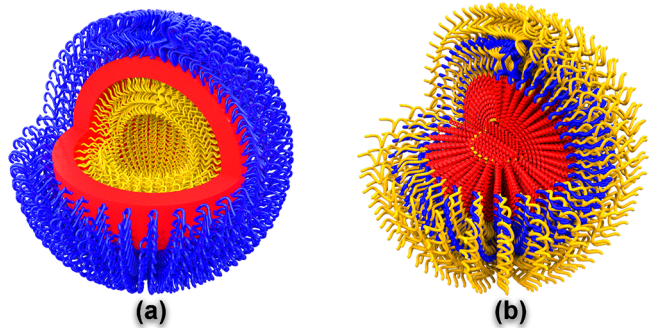

[a] Red is the block P(His-*co*-BLG), blue is PEO, and yellow is PLL.

Scheme 6. Schematic Representation Showing the Curvature of the Hydrophilic−Hydrophobic Interface as Well as the Mixed Coronae of the Obtained Core-Shell Micelles: (a) Branched Polymers and (b) Linear Polymers with Low PLL Molecular Weight[a]

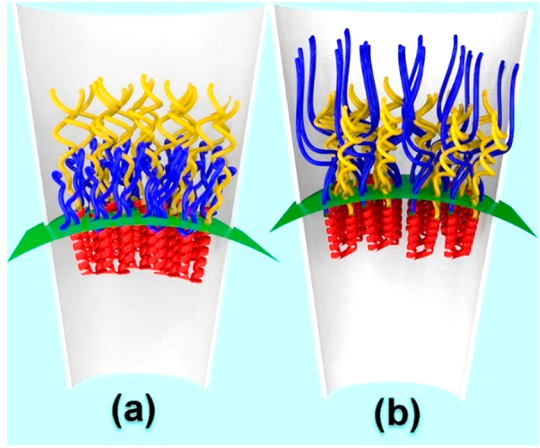

[a] Blue is PEO, red is P(His-*co*-BLG), and yellow is PLL.

DOI: 10.1021/acs.biomac.9b01331
Biomacromolecules XXXX, XXX, XXX−XXX

Scheme 7. Schematic Representation Showing the Interfacial Curvature and Outer vs Inner Hydrophilic Domain Composition of the Obtained Vesicular Nanostructures: (a) Branched Polymers, (b) Linear Polymers, (c, d) Linear Polymers with Flat Interphase, and (e) Branched Polymers[a]

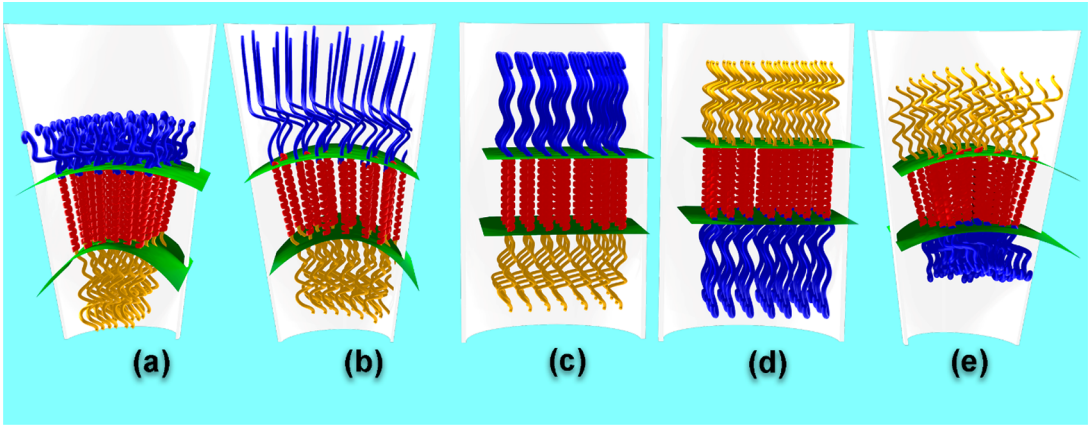

[a]Blue is PEO, red is P(His-*co*-BLG), and yellow is PLL.

chains (Scheme 6a), rendering the zeta potential more positive. On the contrary, in the case of the L15 and S15 pair, the linear L15 polymer structure resulted in spherical core−shell micelles with higher zeta potential than the respective L7 NPs with $M_{n,PLL}$ = 7.0 × 10^3 g mol^{-1} (Scheme 6a).

This is reasonable since the longer PLL blocks are located in the outer periphery in the case of L15 polymer screening the shorter PEO chains, rendering the NPs strongly positively charged (Scheme 6a). Surprisingly, contrary to the linear polymer L15 findings, the 3-miktoarm S15 polymer resulted in the development of vesicular structures (R_G/R_H = 1.02) with zeta-potential values close to 0 mV (+3.8 ± 0.3 mV). This shows that the star-shaped macromolecular architecture cause the interface of the assemblies to curve inward toward the third arm, forcing the branched PEO chains to form the outer hydrophilic layer and the PLL blocks to be located in the inner domain of the polymersomes (Schemes 5a and 7a). In the case of the L25 and S25 pair, light scattering measurements suggest the formation of vesicular structures (R_G/R_H = 1.02 and 0.98, respectively) with positively charged PLL chains located in their outer periphery (Scheme 7d for L25 and 7e for S25).

In this case, the interfacial curvature induced by the 3-arm star macromolecular architecture of the hybrid terpolypeptide cannot maintain the hydrophilic PEO blocks on the outer periphery of the NPs, thereby forcing an outer−inner hydrophilic domain inversion due to the increased length of the PLL blocks that dominates their self-assembly process. In the case of the L45 and S45 polymers, the linear architecture led to the formation of vesicular structures (R_G/R_H = 1.01) with PLL blocks covering their outer periphery and PEO blocks the inner part (Scheme 7d), whereas S45 self-assembled into a core−shell structure (R_G/R_H = 0.78) with a mixed corona composed of both hydrophilic polymers (Scheme 6a). As in the case of L15, since PLL blocks are longer than those of PEO, the positive charge of PLL dominates, resulting in a strong positive surface charge of the NPs, equal to the that of L45 with a pure corona composed only of PLL.

On the basis of our findings, it is obvious that the star-shaped macromolecular architecture resulting in increased PEO density close to the outer interface influenced the structure of the hybrid triblock terpolypeptide, and PEO remained in the outer periphery despite the fact that the PLL block was significantly longer compared to PEO ($M_{n,PEO}$ = 5 × 10^3 g mol^{-1} for the star and $M_{n,PLL}$ = 15 × 10^3 g mol^{-1} for the linear). Therefore, we have demonstrated that it is possible to change the self-assembly behavior and resulting structure of the NPs independently of the relative volume fraction of their hydrophilic block components by altering the macromolecular architecture of the triblock terpolymers from linear to star-shaped.

3.7. pH-Responsiveness of the Not-Loaded NPs. Based on DLS measurements shown in Table 3, it is clear that the empty self-assembled NPs formed by either the linear or the miktoarm star polymers are responsive toward changes in solution pH, owing to gradual protonation of PHis units at lower pH, leading to increased hydrophilicity of the polymers.[54] In particular, at pH = 6.5 (i.e., the extracellular pH value of cancer cells), a small D_h increase was measured in all cases, although the swelling of the assemblies was not very strong. Importantly, upon further lowering of the pH matching the value of the late endosome (pH = 5.0), a significant size increase was monitored in all cases, and the count rate of the aggregates was significantly lowered as compared to the one obtained at pH = 7.4. The observed size changes at different pH values highlight that the formed NPs are significantly swollen at pH = 5.0, and their number is either drastically lowered or the NPs are completely disrupted. The lower values of KCounts at lower pH values, while maintaining the same polymer concentration at all pH solutions indicate that the aggregates not only swell but they also become ruptured.

3.8. Enzymatic Degradation Studies of the Empty NPs. Recently, the utilization of enzymatic degradation of polypeptide-based nanoparticles by proteolytic enzymes has been investigated as an additional advantage of such systems, offering a new stimulus for their drug release applications and establishing biodegradation as an important structural characteristic.[64−66] Cancer cells often secrete proteolytic enzymes that can act as an external stimulus for polypeptide-based materials to gradually release their loaded cargo. Due to the partial polypeptide nature of the NPs developed in the present study, we exploited their responsiveness toward this external stimulus in order to induce the release of their drug cargo. Biodegradation is distinct from this stimulus as a

DOI: 10.1021/acs.biomac.9b01331
Biomacromolecules XXXX, XXX, XXX−XXX

biological process, as it can also be mediated by the normal proteolytic activity of the extracellular matrix. Various enzymes can potentially participate in these biochemical processes. In our case, LAP and trypsin were used for the enzyme degradation studies on the NPs. LAP is an exopeptidase that catalyzes the hydrolysis of amino acid residues only from the amino terminus of polypeptide chains,[67] while trypsin is an endopeptidase which can cleave randomly the amide bonds of lysine residues from their C-terminal side.[68] Thus, free amino groups are produced during the degradation by each enzyme. During the enzyme-mediated degradation reaction of the nanostructures, aliquots were withdrawn at specific time points and were reacted with fluorescamine.[69] The product of this reaction can be detected by fluorescence measurements and can be used to calculate the rate of enzymatic degradation of the NPs. In this study, two distinct phenomena occurred at the same time: one was the reaction of fluorescamine with the exposed ε-amino groups of the PLL blocks, while the second was the reaction of the amines produced due to the degradation of the polypeptides through the catalytic hydrolysis by the two proteases. In the cases that the reaction of fluorescamine with free ε-amino groups of PLL was faster than the reaction of cleaved free amino acids, specific activity measurements were mentioned as "FLUOR". This was determined by studying the coupling reaction with fluorescamine in the absence and in the presence of each enzyme, where the fluorescence was higher when no enzyme was utilized (Table 4). This indicates that the enzymes are not able to react fast enough with the NPs due to steric hindrance that does not allow for increased interactions with the terminal amino groups in the case of LAP or with any polypeptide in the case of trypsin. It should be noticed that LAP is a significantly larger enzyme by volume as compared with trypsin.

Table 4. Biodegradation Evaluation of Empty NPs after Incubation with (a) LAP for 24 h and (b) Trypsin for 1 h at 37 °C

polymer	specific activity of LAP, s^{-1} mg^{-1}NPs	specific activity of trypsin, s^{-1} mg^{-1}NPs
L7	FLUOR	0.10
S7	3.5×10^{-4}	FLUOR
L15	3.9×10^{-4}	FLUOR
S15	1.1×10^{-9} (negligible)	2.1×10^{-7} (negligible)
L25	4.0×10^{-4}	FLUOR
S25	4.5×10^{-4}	FLUOR
L45	3.8×10^{-4}	FLUOR
S45	4.2×10^{-4}	FLUOR

As mentioned above, in the case of the L7 NPs, spherical core−shell micelles are formed with both hydrophilic PEO and PLL chains comprising their outer periphery. Since the PLL chains are shorter than those of PEO, LAP (which can only interact with the terminal ε-amino groups of the PLL) reacts more slowly than fluorescamine since the amino groups are hidden by the PEO chains, while small molecule fluorescamine can penetrate the shell of the PEO chains in a more facile manner. Still, for the same NPs, trypsin can rather rapidly cleave the PLL chains that are located at the outer shell of the NPs even if they are buried within the flexible chains of PEO, and the degradation of PLL is faster than the reaction of the side amine groups with fluorescamine. For the remaining linear and star polymers where the PLL chains are longer and exposed at the outer periphery, trypsin reacts more slowly with the NPs than does fluorescamine.

On the contrary, in the case of S7, where the PEO blocks are shorter than that of PLL and, thus, the PLL chains are more exposed at the shell, LAP reacts rapidly with the end-groups of PLL and cleaves the lysine monomeric units faster than the reaction of fluorescamine with the side groups of PLL. In the case of the L15-S15 pair, the star-based vesicular nanostructures (S15) whose outer periphery is mostly consisted of PEO chains, showed negligible interactions and degradation by both enzymes, contrary to the corresponding linear L15-based chains that showed significantly higher degradation due to the presence of PLL in the mixed corona domain (Scheme 8). It should also be mentioned that the concentration of the proteolytic enzymes used in this study was much higher compared to that present in the organism, and the degradation rate observed is not comparable to those under in vivo conditions, which are expected to be rather slower.

Scheme 8. Schematic Representation Showing that Proteolytic Enzymes (i.e., LAP and Trypsin) can Interact and Degrade the Linear L15-Based Micelles (left), Contrary to the Star-Based S15 Vesicular Analogues (right) That Cannot Be Degraded by the Enzymes Due to the Presence of the Synthetic PEO Located at the Outer Corona

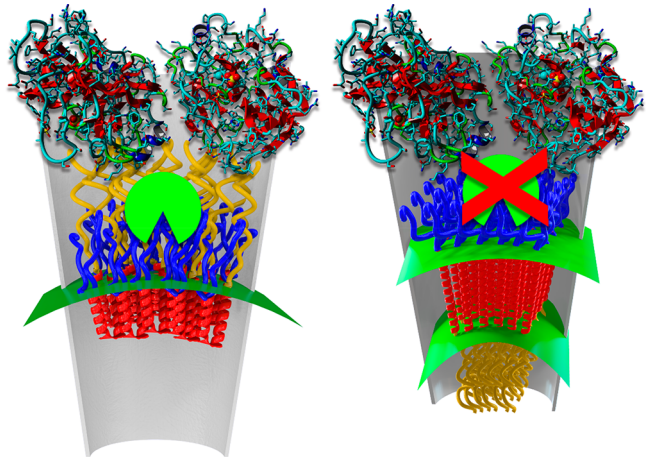

3.9. Self-Assembly of the Everolimus-Loaded Hybrid Triblock Terpolypeptides. The self-assembly behavior of the deprotected hybrid triblock terpolypeptides was subsequently studied upon encapsulation of the anticancer drug Everolimus (EVER) via a solvent-switch methodology similar to that described above. The polymers used for self-assembly and EVER encapsulation were the pairs L15 and S15, as well as L25 and S25. The abbreviation for the polymer NPs with the encapsulated drug are designated as the name of each polymer with the addition of EVER. Therefore, the NPs formed from the self-assembly of linear L15 will designated as L15-EVER. The drug-loaded NPs formed were characterized by DLS, SLS, cryo-TEM, as well as 3D-tomography. Drug release curves at various pH values were performed for the pair L15-EVER and S15-EVER.

3.10. Characteristics of the Drug-Loaded NPs Obtained by Light Scattering and Electrophoretic Mobility Analysis. The dimensions of the Everolimus-loaded L15-S15 and L25-S25 NPs measured by dynamic and static

DOI: 10.1021/acs.biomac.9b01331
Biomacromolecules XXXX, XXX, XXX−XXX

Table 5. Summary of Characteristics of the Everolimus-Loaded Self-Assembled Nanostructures at Different pH Values at 37 °C

polymer	diameter, D_h[a] (nm; 90°), pH = 7.4	diameter, D_h[a] (nm; 90°), pH = 6.5	diameter, D_h[a] (nm; 90°), pH = 5.0	zeta-potential (mV),[b] pH = 7.4	R_G/R_H,[c] pH = 7.4
L15-EVER	205 ± 3	291 ± 4	430 ± 6	+5.0 ± 0.4	1.10
S15-EVER	250 ± 4	330 ± 4	450 ± 6	+4.2 ± 0.3	1.08
L25-EVER	230 ± 4	301 ± 4	510 ± 6	+6.3 ± 0.5	1.10
S25-EVER	369 ± 5	490 ± 6	616 ± 9	+6.1 ± 0.5	1.07

[a]D_h values measured from DLS analysis (the error shows the standard deviation from five repeat measurements). [b]Zeta-potential values measured from microelectrophoretic analysis at pH = 7.4. [c]R_G/R_H ratio determined from SLS and DLS analysis.

light scattering, as well as their zeta potential measured by microelectrophoretic analysis are shown in Table 5. The structure of the drug-loaded NPs is the result of the interactions between the hybrid amphiphilic terpolypeptide, the encapsulated drug and buffer. The obtained characterization results indicate that since the R_G/R_H value determined for all drug-loaded NPs formed is close to 1.00, formation of hollow vesicular structures was expected. In both amphiphilic polymer pairs, the star-shaped polymer precursors form aggregates larger than the corresponding linear ones. In particular, in the case of the polymers with $M_{n,PLL} = 25 \times 10^3$ g mol^{-1}, D_h values of the NPs prepared upon self-assembly of the star polymer are nearly double compared to the corresponding NPs formed by the linear triblock quarterpolymers with the same molecular weight of PLL. For the L15-EVER-S15-EVER pair, the dimensions of the NPs are comparable, although the NPs resulting from the 3-miktoarm star polymers are larger and ellipsoidal than the corresponding NPs composed of the linear polymers. This difference is most possibly attributed to the higher interfacial curvature between the outer corona- and core-forming blocks, which compensates for the larger volume fraction of the PLL block, resulting in a flatter interface and is expected to result to afford NPs with larger dimensions for the star polymers. The encapsulation of the hydrophobic drug Everolimus is expected to increase the thickness of the membrane of vesicles of the hydrophobic domains, that is, the P(His-*co*-BLG) block along with the encapsulated drug. It is obvious that the dimensions of the formed NPs are significantly influenced by the macromolecular architecture of the polymeric materials. As in the case of the empty nanostructures, the pH-responsiveness of the drug-loaded NPs was also investigated by DLS analysis. Significant increase of D_h values was measured in all cases upon lowering the pH value from 7.4 to 6.5 (Table 5), which was more evident upon further pH decrease to 5.0, showing that pH can be successfully utilized as an externally controlled stimulus for the swelling of the synthesized NPs and induction of a pH-regulated drug release (Figure 1). Importantly, since measured zeta potential values were close to 0 mV, it can be concluded that the inert PEO blocks are always located at the outer periphery of the prepared NPs.

3.11. Cryo-TEM Imaging and 3D-Tomography Analysis. Cryo-TEM imaging as well as Cryo-TEM 3d-tomography analysis was performed in order to determine the self-assembly behavior of the NPs in aqueous media. Surprisingly, cryo-TEM images revealed that the nanoassemblies formed by the L25-EVER and S25-EVER, as well as L15-EVER amphiphilic triblock quarterpolymers, were similar in structure but had different overall dimensions. They all formed characteristic "stomatocyte" morphologies not identical but similar to the one found by the group of van Hest[70] who first reported this

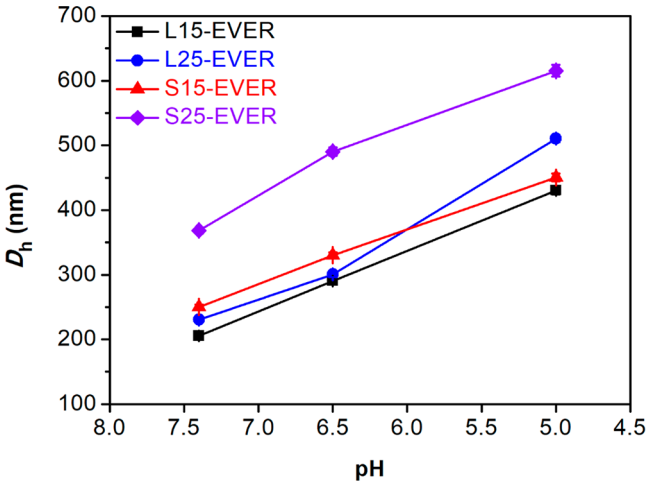

Figure 1. Dependence of the dimensions of the loaded NPs S25-EVER, L25-EVER, L15-EVER, and S15-EVER as a function of pH.

structure, which have been very rarely reported and have only been thoroughly investigated in recent works.[70−78] The corresponding cryo-TEM images are shown in Figure 2a−c. After careful observation, it is evident that almost all of self-assembled NPs present the "stomatocyte" structure, indicating that this is a thermodynamically favorable equilibrium structure rather than a metastable phase (the completely spherical structure observed in one NP is probably due to the fact that it is turned in such a way that the missing part is hidden). It should be also mentioned that the structures remained stable and intact for a period of five weeks. Cryo-TEM imaging observations were in good agreement with DLS and SLS results, where an $R_G/R_H \sim 1.0$ was calculated, indicating that the NPs possess a hollow cavity in their interior structure (Scheme 9).

As shown in the schematic representation of the stomatocytes in Scheme 9, the externally located blue chains represent the hydrophilic PEO blocks, the red and green blended domain represents the hydrophobic P(His-*co*-BLG) copolypeptide containing the encapsulated drug Everolimus, while the inner yellow chains represent the PLL blocks.

Even more surprisingly, the NPs formed by the self-assembly of S15-EVER revealed a "suprapolymersome" morphology with triple-multi-compartmentalized or patchy internal structure. To further investigate this intriguing morphology, cryo-TEM 3D-tomographic analysis of these NPs was conducted to obtain a more detailed characterization of their internal structure. The acquired 3D-tomography images at different tilt angles and slices along the Z axis are shown in Figure 3 (also see Video File S1, SI).

DOI: 10.1021/acs.biomac.9b01331
Biomacromolecules XXXX, XXX, XXX−XXX

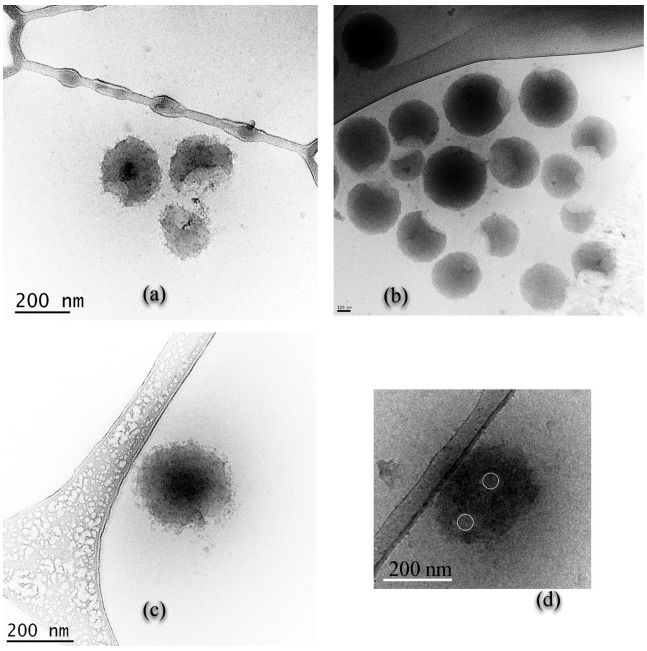

Figure 2. Self-assembled nanostructures with intriguing morphologies formed upon loading of Everolimus: (a) stomatocytes obtained from the L25-EVER, (b) stomatocytes obtained from the S25-EVER, (c) stomatocytes obtained from the L15-EVER, and (d) supramolecular polymersomes from the S15-EVER, as projected perpendicular to axis *Z* (see also Figure 3). Better views of its structure can be obtained from the two video files, Video Files S1 and S2 in the SI.

Scheme 9. Schematic Representation of the Suggested Internal Microphase-Separated Structure of the Formed Drug-Loaded Stomatocytes

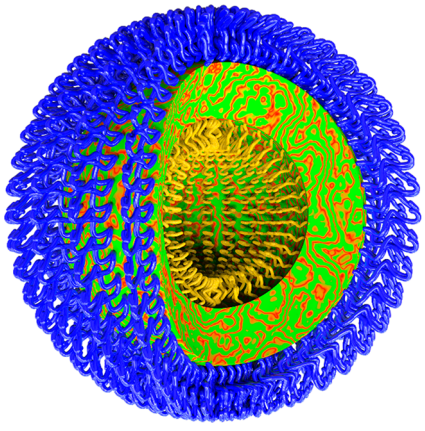

The two circles in Figure 3a indicate the beginning of the development of the two cylinders, shown in perpendicular projection to *Z* axis in Figure 2d. In Figure 3b, it can also be seen the development of the third ellipsoidal compartment between the two cylinders. A better view can be obtained in the two video files provided in the SI, Video Files S1 and S2. In particular, the internal hollow space of the nanostructures is composed of three different parts: two well-defined parallel hollow cylinders connected together with another well-defined hollow part with an ellipsoidal shape on the same plane to the cylinders. The two well-defined cylinders can be seen in Figure 2d highlighted with two white circles (see also Video File S2, SI). The diameter of each cylinder is approximately 42 nm, while its length is approximately 255 nm (the longer

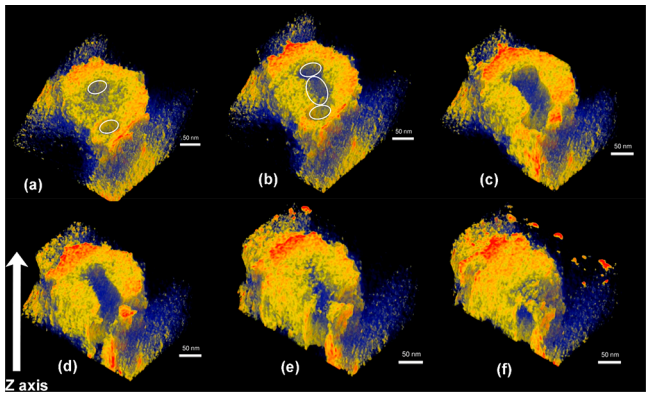

Figure 3. Cryo-TEM 3D-tomography slices of the S15-EVER "suprapolymersome" nanoparticles obtained along the *Z* axis. Slices progress from lower *Z* axis values at (a) to higher *Z* axis values at (f). The white circles and the ellipsoid shows the cavities within the aggregate. The two white circles at (a) indicate the development of the cylinders, shown also on Figure 2d.

dimension). The schematic representation of the dissected S15-EVER-based multicompartmentalized "suprapolymersomes" showing their internal microphase structure, according to the 3D tomography analysis, is depicted in Scheme 10.

Scheme 10. Schematic Representation of the Dissected S15-EVER-Based Multicompartmentalized "Suprapolymersomes"[a]

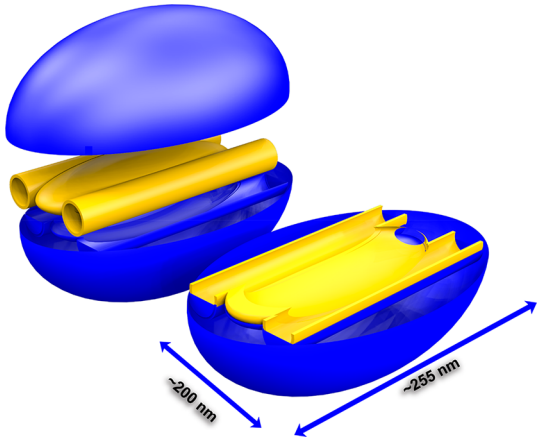

[a] *Z*-axis shown on Figure 3 is the one indicated by 255 nm in this figure.

As shown in Scheme 10, the blue domain represents the polymeric part together with the encapsulated drug, while the yellow domain represents the well-defined empty space within the NP. Since it was not possible to separately stain each material to obtain the internal structure of this particular NP of the PLL, PEO, or of the P(His-*co*-BLG) phases without destroying its structure, it is not possible to separately illustrate each microphase.

It is evident that Everolimus is directing the self-assembly of the polymer−drug mixture in an aqueous environment, since the aggregates obtained in the presence of EVER are completely different from the ones obtained by the polymers alone. This may be due to the large amount of the encapsulated drug which makes it the main component of the aggregates in the EVER-POLYMER mixture and,

DOI: 10.1021/acs.biomac.9b01331
Biomacromolecules XXXX, XXX, XXX−XXX

particularly, of the hydrophobic parts, which direct self-assembly. As discussed in the next session, EVER presented a loading content of 25% per weight of the total L15 and S15 polymers. At these polymers, the hydrophobic part (PHis-*co*-PBLG at pH = 7.4) is only 17.5% (w/w) of the mixture and EVER is 20%, where PLL is 37.5% (w/w) and PEO is 25% (w/w). Between the hydrophobic parts of the mixture, EVER is 53% (w/w). Therefore, it is obvious that EVER drives the self-assembly of these NPs. The fact that self-assembly is directed in both stomatocytes, as well as the supramolecular polymersomes, might also be due to the large molecular weight of the drug, as well as the peculiar structure of EVER, which is a cyclic molecule with a "tail" (Scheme 11) that might induce

Scheme 11. Structure of the Anticancer Drug Everolimus

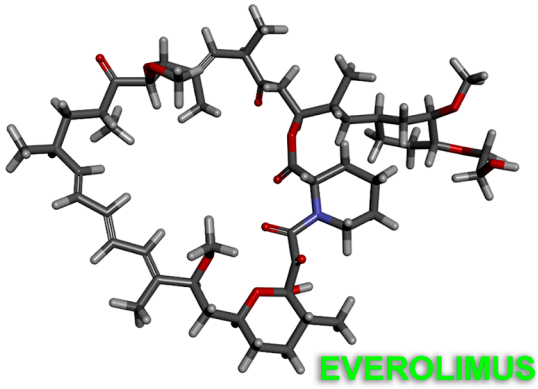

steric hindrances and the interaction with the complex structure of the polymer affords these structures. Non-spherical toroidal structures have been obtained from the self-assembly through electrostatic interactions between a plasmid DNA and PLL, where the cyclic and high molecular weight of DNA molecule directed the self-assembly of the polyplexes. Probably the similar cyclic structure of Everolimus directed to the formation of these non-spherical structures observed at this work.[79]

3.12. Drug Loading and In Vitro Release Studies. EVER is a rather new anticancer agent that was approved by the FDA in 2011 for the treatment of progressive pancreatic neuroendocrine tumors.[80,81] It is a rapamycin mTOR inhibitor that exhibits antitumor activity via disruption of various signaling pathways and it is also used in the treatment of advanced renal cell cancer, breast cancer and neuroendocrine tumors (NET); as well as an antirejection agent for transplantation.[82] Lipid disorders, hyperglycemia as well as increase of LDL cholesterol have emerged as common and unique side effects upon treatment with EVER.[83,84] Therefore, it is necessary for the drug to be delivered through a nanoparticulate drug delivery system in order to control its release behavior and biodistribution, and avoid undesired side effects.

EVER is rather hydrophobic and interacts with the P(His-*co*-BLG) block through $\pi-\pi$ interactions via the phenyl groups of the drug and BLG units. In order to determine the optimum polymer-to-drug weight ratio, the amount of the polymer used was kept constant, whereas the amount of EVER was varied during the drug encapsulation process. It was found that 10 mg of either L15 or S15 and 3 mg of drug gave the optimum drug loading efficiency (83.3% w/w) and loading content (25.0% w/w). By increasing the initial Everolimus/polymer ratio, it was found that the drug loading remained constant, while the loading efficiency progressively decreased, therefore the developed NPs had the capability to encapsulate a certain amount of Everolimus while the remainder of the drug precipitated since it is insoluble in water. To the best of our knowledge, there only report of the nanoparticulate delivery of EVER, is a paper by Houdaihed et al.[85] In this study, EVER was encapsulated into polymeric NPs based on a poly(ethylene glycol)-*b*-poly(lactide-*co*-glycolide) copolymer, with 9.1% drug loading and 41% loading efficiency. The low loading efficiency found by Houdaihed et al.[85] is most possibly attributed to the lack of aromatic bonds in the polymer structure and therefore to the absence of $\pi-\pi$ interactions developed between the polymer and the drug. The nanoparticles synthesized in our work remained stable under storage conditions at 37 °C for at least 12 h in a 10% FBS containing buffer.

In vitro drug release studies for the L15-EVER-S15-EVER NP pair at different pH values revealed the pH-responsive character of the developed nanostructures. The PHis homopolymer has a pK_a of 6.5 that varies slightly depending on its molecular weight. If instead of the P(His-*co*-BLG) middle block, a PHis homopolymer of the same molecular weight was incorporated in the synthesized triblock terpolymers, almost quantitative drug release could have been achieved at pH = 6.5 (i.e., pH value similar to the extracellular pH value of cancer cells). On the contrary, upon introduction of the BLG groups, the pK_a of the polymer was reduced to 6.1,[54] and thus, a limited drug release (<30%) was achieved in both cases over a 140 h period at the extracellular cancer cell pH value. Moreover, this finding agreed well with the drug release profile of both NPs where near quantitative pH-triggered drug release (>80%) occurred at the late endosome intracellular pH (pH = 5.0), as shown in Figure 4. It should be mentioned that the drug lacks pH responsiveness; therefore, the release is due exclusively to the pH-responsiveness of polyhistidine. The similar release profile between the two NPs may be due to the fact that the release is based on the transformation of PHis.

4. CONCLUSION

In order to design an effective polymeric drug delivery system, it is necessary to control several characteristics of the carrier, such as its functionality, size, shape, and mechanical properties, as well as its surface functionality. Therefore, it would be possible to fine-tune the self-assembly behavior of the amphiphilic polymers that form the drug delivery vehicle. In the present study, we have shown that the key parameters that define the aggregation of block copolymer amphiphiles are not only the polymer−polymer and polymer−solvent interactions as well as the composition of each polymeric block, but also their macromolecular architecture. A series of stimuli-responsive 3-miktoarm star amphiphilic hybrid triblock terpolypeptides and their corresponding linear analogues were synthesized exhibiting the same molecular characteristics but different macromolecular architecture, and their self-assembly in aqueous media was investigated. It was shown that, for amphiphilic polymers exhibiting identical molecular characteristics, the macromolecular architecture could completely alter not only the overall dimensions but also the morphology of the developed nanoparticles, defining whether the polypeptide-based amphiphiles would self-assemble into a core−shell micelle or a vesicular structure.

DOI: 10.1021/acs.biomac.9b01331
Biomacromolecules XXXX, XXX, XXX−XXX

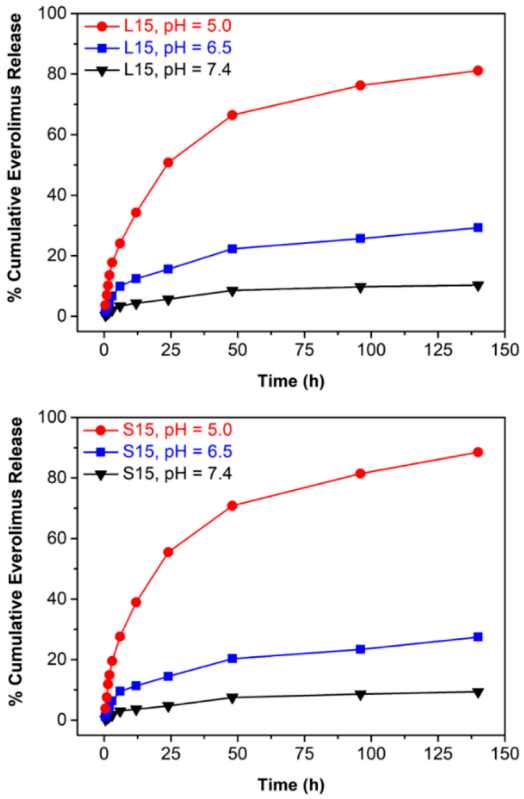

Figure 4. Cumulative Everolimus release curves at different pH values, from L15-EVER and S15-EVER, showing a clear pH-dependent drug release behavior of both NPs.

By performing enzymatic degradation studies, we showed that the star-shaped architecture also increased the stability of the nanoparticles toward protease degradation as compared to the linear architecture, particularly when PEO was in their outer periphery, since the degradation of PEO by enzymes is relatively slow. This was expected in the case of the NPs that were formed from linear polymers, since the cleavage of the one-arm PEO block is critical for the self-assembly of the remaining copolymer, while in the case of the star architecture the cleavage of one PEO chain is not as disruptive since there is a second PEO block for stabilization of the assemblies. This finding is expected to result in increased stability of the 3-miktoarm star polymer-based NPs within the blood compartment and should increase its probability to reach and accumulate at cancer cells via a passive or an active targeting mechanism. Importantly, encapsulation of the anticancer drug Everolimus was achieved into the nanostructures formed from either the 3-miktoarm star triblock terpolypeptides or their linear counterparts with high loading efficiencies, where in the former case two intriguing non-spherical NP morphologies were observed (i.e., "stomatocytes" similar but not identical to the ones reported by the group of van Hest[70] and "multi-compartmentalized superpolymersomes"). The structure of the developed "stomatocytes" was similar to but smaller than red blood cells, which have the ability to bypass the hemorheological barriers within the blood compartment and show increased cellular uptake properties. In addition, the artificially shaped red blood cells prepared in our study showed excellent pH-responsive properties within physiological values for the controlled release of Everolimus. The drug presented minimum release at pH = 7.4, while at extracellular pH of cancer cells (pH = 6.5) it showed a slow release rate that was maximized at intracellular late endosome pH values (pH = 5.0). In future studies, we intend to perform in vivo assays against human pancreatic cancer xenografts to evaluate their effectiveness. Finally, we believe that the ongoing synergy of materials and pharmaceutical scientists, biologists, and clinical oncologists is imperative to produce efficient drug delivery systems that possess advanced properties and required functionalities to fight pancreatic cancer.

■ ASSOCIATED CONTENT

Supporting Information

The Supporting Information is available free of charge on the ACS Publications website at DOI: 10.1021/acs.biomac.9b01331.

Figures S1−S3: Characterization results of the NCAs and the polymers; Schemes S1−S2: Polymerization apparatus, molecular structure of the enzymes; Figures S4−S27: DLS curves (PDF)

Video File S1 Suprapolymersome: 3D tomography of the suprapolymersome (MPG)

Video File S2 Tilted Suprapolymersome: Tilted suprapolymersome (MPG)

■ AUTHOR INFORMATION

Corresponding Author

*E-mail: iatrou@chem.uoa.gr.

ORCID

Panayiotis Bilalis: 0000-0002-5809-9643
Spyridon Varlas: 0000-0002-4171-7572
Efstratios Stratikos: 0000-0002-3566-2309
Olli Ikkala: 0000-0002-0470-1889
Hermis Iatrou: 0000-0001-9358-0769

Author Contributions

†These authors contributed equally to this work. The manuscript was written through contributions of all authors. All authors have given approval to the final version of the manuscript.

Notes

The authors declare no competing financial interest.

■ ACKNOWLEDGMENTS

The present work was cofunded by the European Union and Greek national funds through the Operational Program "Competitiveness, Entrepreneurship, and Innovation", under the call "RESEARCH-CREATE-INNOVATE" (Acronym: LIPODOX, Project Code: T1EDK-01833).

■ REFERENCES

(1) Safra, T.; Muggia, F.; Jeffers, S.; Tsao-Wei, D. D.; Groshen, S.; Lyass, O.; Henderson, R.; Berry, G.; Gabizon, A. Pegylated liposomal doxorubicin (doxil): reduced clinical cardiotoxicity in patients reaching or exceeding cumulative doses of 500 mg/m2. *Ann. Oncol.* **2000**, *11* (8), 1029−1033.

(2) Barenholz, Y. Doxil - The first FDA-approved nano-drug: Lessons learned. *J. Controlled Release* **2012**, *160* (2), 117−134.

(3) Hawkins, M. J.; Soon-Shiong, P.; Desai, N. Protein nanoparticles as drug carriers in clinical medicine. *Adv. Drug Delivery Rev.* **2008**, *60* (8), 876−885.

(4) Ferrari, M. Frontiers in cancer nanomedicine: Directing mass transport through biological barriers. *Trends Biotechnol.* **2010**, *28* (4), 181−188.

DOI: 10.1021/acs.biomac.9b01331
Biomacromolecules XXXX, XXX, XXX−XXX

(5) Mura, S.; Nicolas, J.; Couvreur, P. Stimuli-responsive nanocarriers for drug delivery. *Nat. Mater.* **2013**, *12* (11), 991−1003.
(6) Bilalis, P.; Skoulas, D.; Karatzas, A.; Marakis, J.; Stamogiannos, A.; Tsimblouli, C.; Sereti, E.; Stratikos, E.; Dimas, K.; Vlassopoulos, D.; Iatrou, H. Self-Healing pH- and Enzyme Stimuli-Responsive Hydrogels for Targeted Delivery of Gemcitabine To Treat Pancreatic Cancer. *Biomacromolecules* **2018**, *19* (9), 3840−3852.
(7) Skoulas, D.; Christakopoulos, P.; Stavroulaki, D.; Santorinaios, K.; Athanasiou, V.; Iatrou, H. Micelles formed by polypeptide containing polymers synthesized via N-carboxy anhydrides and their application for cancer treatment. *Polymers* **2017**, *9* (6), 208−253.
(8) Liarou, E.; Varlas, S.; Skoulas, D.; Tsimblouli, C.; Sereti, E.; Dimas, K.; Iatrou, H. Smart polymersomes and hydrogels from polypeptide-based polymer systems through α-amino acid N-carboxyanhydride ring-opening polymerization. From chemistry to biomedical applications. *Prog. Polym. Sci.* **2018**, *83*, 28−78.
(9) Bertrand, N.; Wu, J.; Xu, X.; Kamaly, N.; Farokhzad, O. C. Cancer nanotechnology: The impact of passive and active targeting in the era of modern cancer biology. *Adv. Drug Delivery Rev.* **2014**, *66*, 2−25.
(10) Hui, Y.; Yi, X.; Hou, F.; Wibowo, D.; Zhang, F.; Zhao, D.; Gao, H.; Zhao, C.-X. Role of Nanoparticle Mechanical Properties in Cancer Drug Delivery. *ACS Nano* **2019**, *13* (7), 7410−7424.
(11) Gentile, F.; Chiappini, C.; Fine, D.; Bhavane, R. C.; Peluccio, M. S.; Cheng, M. M.-C.; Liu, X.; Ferrari, M.; Decuzzi, P. The effect of shape on the margination dynamics of non-neutrally buoyant particles in two-dimensional shear flows. *J. Biomech.* **2008**, *41* (10), 2312−2318.
(12) Champion, J. A.; Mitragotri, S. Role of target geometry in phagocytosis. *Proc. Natl. Acad. Sci. U. S. A.* **2006**, *103* (13), 4930−4934.
(13) Wang, G.; Inturi, S.; Serkova, N. J.; Merkulov, S.; McCrae, K.; Russek, S. E.; Banda, N. K.; Simberg, D. High-Relaxivity Superparamagnetic Iron Oxide Nanoworms with Decreased Immune Recognition and Long-Circulating Properties. *ACS Nano* **2014**, *8* (12), 12437−12449.
(14) Park, J.-H.; von Maltzahn, G.; Zhang, L.; Derfus, A. M.; Simberg, D.; Harris, T. J.; Ruoslahti, E.; Bhatia, S. N.; Sailor, M. J. Systematic surface engineering of magnetic nanoworms for in vivo tumor targeting. *Small* **2009**, *5* (6), 694−700.
(15) Geng, Y.; Dalhaimer, P.; Cai, S.; Tsai, R.; Tewari, M.; Minko, T.; Discher, D. E. Shape effects of filaments versus spherical particles in flow and drug delivery. *Nat. Nanotechnol.* **2007**, *2* (4), 249−255.
(16) Christian, D. A.; Cai, S.; Garbuzenko, O. B.; Harada, T.; Zajac, A. L.; Minko, T.; Discher, D. E. Flexible Filaments for in Vivo Imaging and Delivery: Persistent Circulation of Filomicelles Opens the Dosage Window for Sustained Tumor Shrinkage. *Mol. Pharmaceutics* **2009**, *6* (5), 1343−1352.
(17) Huang, X.; Li, L.; Liu, T.; Hao, N.; Liu, H.; Chen, D.; Tang, F. The Shape Effect of Mesoporous Silica Nanoparticles on Biodistribution, Clearance, and Biocompatibility in Vivo. *ACS Nano* **2011**, *5* (7), 5390−5399.
(18) Arnida; Janat-Amsbury, M.M.; Ray, A.; Peterson, C.M.; Ghandehari, H. Geometry and surface characteristics of gold nanoparticles influence their biodistribution and uptake by macrophages. *Eur. J. Pharm. Biopharm.* **2011**, *77* (3), 417−423.
(19) Zhou, Z.; Ma, X.; Jin, E.; Tang, J.; Sui, M.; Shen, Y.; Van Kirk, E. A.; Murdoch, W. J.; Radosz, M. Linear-dendritic drug conjugates forming long-circulating nanorods for cancer-drug delivery. *Biomaterials* **2013**, *34* (22), 5722−5735.
(20) Godin, B.; Chiappini, C.; Srinivasan, S.; Alexander, J. F.; Yokoi, K.; Ferrari, M.; Decuzzi, P.; Liu, X. Drug Delivery: Discoidal Porous Silicon Particles: Fabrication and Biodistribution in Breast Cancer Bearing Mice. *Adv. Funct. Mater.* **2012**, *22* (20), 4225−4235.
(21) Muro, S.; Garnacho, C.; Champion, J. A.; Leferovich, J.; Gajewski, C.; Schuchman, E. H.; Mitragotri, S.; Muzykantov, V. R. Control of Endothelial Targeting and Intracellular Delivery of Therapeutic Enzymes by Modulating the Size and Shape of ICAM-1-targeted Carriers. *Mol. Ther.* **2008**, *16* (8), 1450−1458.
(22) Wilhelm, S.; Tavares, A. J.; Dai, Q.; Ohta, S.; Audet, J.; Dvorak, H. F.; Chan, W. C. W. Analysis of nanoparticle delivery to tumours. *Nat. Rev. Mater.* **2016**, *1* (5), 16014−16026.
(23) Gradishar, W. J.; Tjulandin, S.; Davidson, N.; Shaw, H.; Desai, N.; Bhar, P.; Hawkins, M.; O'Shaughnessy, J. Phase III trial of nanoparticle albumin-bound paclitaxel compared with polyethylated castor oil-based paclitaxel in women with breast cancer. *J. Clin. Oncol.* **2005**, *23* (31), 7794−7803.
(24) O'Brien, M. E. R.; Wigler, N.; Inbar, M.; Rosso, R.; Grischke, E.; Santoro, A.; Catane, R.; Kieback, D. G.; Tomczak, P.; Ackland, S. P.; Orlandi, F.; Mellars, L.; Alland, L.; Tendler, C. Reduced cardiotoxicity and comparable efficacy in a phase III trial of pegylated liposomal doxorubicin HCl (CAELYX/Doxil) versus conventional doxorubicin for first-line treatment of metastatic breast cancer. *Ann. Oncol.* **2004**, *15* (3), 440−449.
(25) Caliceti, P.; Veronese, F. M. Pharmacokinetic and biodistribution properties of poly(ethylene glycol)-protein conjugates. *Adv. Drug Delivery Rev.* **2003**, *55* (10), 1261.
(26) Wu, W.; Wang, W.; Li, J. Star polymers: Advances in biomedical applications. *Prog. Polym. Sci.* **2015**, *46*, 55−85.
(27) Gu, Z.; Gao, D.; Al-Zubaydi, F.; Li, S.; Singh, Y.; Rivera, K.; Holloway, J.; Szekely, Z.; Love, S.; Sinko, P. J. The effect of size and polymer architecture of doxorubicin-poly(ethylene) glycol conjugate nanocarriers on breast duct retention, potency and toxicity. *Eur. J. Pharm. Sci.* **2018**, *121*, 118−125.
(28) Kakkar, A.; Traverso, G.; Farokhzad, O. C.; Weissleder, R.; Langer, R. Evolution of macromolecular complexity in drug delivery systems. *Nat. Rev. Chem.* **2017**, *1* (8), 0063.
(29) Iatrou, H.; Hadjichristidis, N. Synthesis of a model 3-miktoarm star terpolymer. *Macromolecules* **1992**, *25* (18), 4649−4651.
(30) Hadjichristidis, N.; Pitsikalis, M.; Pispas, S.; Iatrou, H. Polymers with Complex Architecture by Living Anionic Polymerization. *Chem. Rev.* **2001**, *101* (12), 3747−3792.
(31) Park, J.; Jang, S.; Kon Kim, J. Morphology and microphase separation of star copolymers. *J. Polym. Sci., Part B: Polym. Phys.* **2015**, *53* (1), 1−21.
(32) Hadjichristidis, N.; Iatrou, H.; Behal, S. K.; Chludzinski, J. J.; Disko, M. M.; Garner, R. T.; Liang, K. S.; Lohse, D. J.; Milner, S. T. Morphology and miscibility of miktoarm styrene-diene copolymers and terpolymers. *Macromolecules* **1993**, *26* (21), 5812−5815.
(33) Iatrou, H.; Siakali-Kioulafa, E.; Hadjichristidis, N.; Roovers, J.; Mays, J. Hydrodynamic properties of model 3-miktoarm star copolymers. *J. Polym. Sci., Part B: Polym. Phys.* **1995**, *33* (13), 1925−1932.
(34) Iatrou, H.; Willner, L.; Hadjichristidis, N.; Halperin, A.; Richter, D. Aggregation Phenomena of Model PS/PI Super-H-Shaped Block Copolymers. Influence of the Architecture. *Macromolecules* **1996**, *29* (2), 581−591.
(35) Junnila, S.; Houbenov, N.; Hanski, S.; Iatrou, H.; Hirao, A.; Hadjichristidis, N.; Ikkala, O. Hierarchical Smectic Self-Assembly of an ABC Miktoarm Star Terpolymer with a Helical Polypeptide Arm. *Macromolecules* **2010**, *43* (21), 9071−9076.
(36) Karatzas, A.; Iatrou, H.; Hadjichristidis, N.; Inoue, K.; Sugiyama, K.; Hirao, A. Complex Macromolecular Chimeras. *Biomacromolecules* **2008**, *9* (7), 2072−2080.
(37) Osada, K.; Cabral, H.; Mochida, Y.; Lee, S.; Nagata, K.; Matsuura, T.; Yamamoto, M.; Anraku, Y.; Kishimura, A.; Nishiyama, N.; Kataoka, K. Bioactive Polymeric Metallosomes Self-Assembled through Block Copolymer-Metal Complexation. *J. Am. Chem. Soc.* **2012**, *134* (32), 13172−13175.
(38) Huang, J.; Liang, H.; Cheng, D.; Lu, J. Polypeptide−poly(ethylene glycol) miktoarm star copolymers with a fluorescently labeled core: synthesis, delivery and imaging of siRNA. *Polym. Chem.* **2016**, *7*, 1792−1802.
(39) Babin, J.; Leroy, C.; Lecommandoux, S.; Borsali, R.; Gnanou, Y.; Taton, D. Towards an easy access to amphiphilic rod-coil miktoarm star copolymers. *Chem. Commun.* **2005**, *15*, 1993−1995.
(40) Babin, J.; Taton, D.; Brinkmann, M.; Lecommandoux, S. Synthesis and Self-Assembly in Bulk of Linear and Mikto-Arm Star

DOI: 10.1021/acs.biomac.9b01331
Biomacromolecules XXXX, XXX, XXX−XXX

Block Copolymers Based on Polystyrene and Poly(glutamic acid). *Macromolecules* **2008**, *41* (4), 1384−1392.
(41) Hadjichristidis, N.; Iatrou, H.; Pispas, S.; Pitsikalis, M. Anionic polymerization: High vacuum techniques. *J. Polym. Sci., Part A: Polym. Chem.* **2000**, *38* (18), 3211−3234.
(42) Mastronarde, D. N. Automated electron microscope tomography using robust prediction of specimen movements. *J. Struct. Biol.* **2005**, *152* (1), 36−51.
(43) Kremer, J. R.; Mastronarde, D. N.; McIntosh, J. R. Computer visualization of three-dimensional image data using IMOD. *J. Struct. Biol.* **1996**, *116* (1), 71−76.
(44) Engelhardt, P. Electron Tomography of Chromosome Structure. *Encyclopedia of Analytical Chemistry*; John Wiley & Sons, Ltd., 2006.
(45) Jensen, T. L.; Jørgensen, H. J.; Hansen, C. P.; Jensen, H. S. Implementation of an optimal first-order method for strongly convex total variation regularization. *BIT Numerical Mathematics* **2012**, *52* (2), 329−356.
(46) Palenstijn, W. J.; Batenburg, K. J.; Sijbers, J. Performance improvements for iterative electron tomography reconstruction using graphics processing units (GPUs). *J. Struct. Biol.* **2011**, *176* (2), 250−253.
(47) van Aarle, W.; Palenstijn, W. J.; De Beenhouwer, J.; Altantzis, T.; Bals, S.; Batenburg, K. J.; Sijbers, J. The ASTRA Toolbox: A platform for advanced algorithm development in electron tomography. *Ultramicroscopy* **2015**, *157*, 35−47.
(48) Hall, M.; Frank, E.; Holmes, G.; Pfahringer, B.; Reutemann, P.; Witten, H. The WEKA Data Mining Software: An Update. *SIGKDD Explorations* **2009**, *11*, 1−9.
(49) Elbert, D. L.; Hubbell, J. A. Conjugate Addition Reactions Combined with Free-Radical Cross-Linking for the Design of Materials for Tissue Engineering. *Biomacromolecules* **2001**, *2* (2), 430−441.
(50) Hadjichristidis, N.; Iatrou, H.; Pitsikalis, M.; Sakellariou, G. Synthesis of Well-Defined Polypeptide-Based Materials via the Ring-Opening Polymerization of alpha-Amino Acid N-Carboxyanhydrides. *Chem. Rev.* **2009**, *109* (11), 5528−5578.
(51) Aliferis, T.; Iatrou, H.; Hadjichristidis, N. Living polypeptides. *Biomacromolecules* **2004**, *5* (5), 1653−1656.
(52) Iatrou, H.; Frielinghaus, H.; Hanski, S.; Ferderigos, N.; Ruokolainen, J.; Ikkala, O.; Richter, D.; Mays, J.; Hadjichristidis, N. Architecturally induced multiresponsive vesicles from well-defined polypeptides. Formation of gene vehicles. *Biomacromolecules* **2007**, *8* (7), 2173−2181.
(53) Mondeshki, M.; Spiess, H. W.; Aliferis, T.; Iatrou, H.; Hadjichristidis, N.; Floudas, G. Hierarchical self-assembly in diblock copolypeptides of poly(gamma-benzyl-L-glutamate) with poly(L-leucine) and poly(O-benzyl-L-tyrosine). *Eur. Polym. J.* **2011**, *47* (4), 668−674.
(54) Mavrogiorgis, D.; Bilalis, P.; Karatzas, A.; Skoulas, D.; Fotinogiannopoulou, G.; Iatrou, H. Controlled polymerization of histidine and synthesis of well-defined stimuli responsive polymers. Elucidation of the structure-aggregation relationship of this highly multifunctional material. *Polym. Chem.* **2014**, *5* (21), 6256−6278.
(55) Huber, V.; Camisaschi, C.; Berzi, A.; Ferro, S.; Lugini, L.; Triulzi, T.; Tuccitto, A.; Tagliabue, E.; Castelli, C.; Rivoltini, L. Cancer acidity: An ultimate frontier of tumor immune escape and a novel target of immunomodulation. *Semin. Cancer Biol.* **2017**, *43*, 74−89.
(56) Hu, Y.-B.; Dammer, E. B.; Ren, R.-J.; Wang, G. The endosomal-lysosomal system: from acidification and cargo sorting to neurodegeneration. *Transl. Neurodegener.* **2015**, *4*, 18−28.
(57) Schwyzer, R.; Rittel, W. Synthese von Peptid-Zwischenprodukten für den Aufbau eines corticotrop wirksamen Nonadecapeptids. I. Nε-t-Butyloxycarbonyl-L-lysin, Nε-(Nε-t-Butyloxycarbonyl-L-lysyl)-Nε-t-butyloxycarbonyl-L-lysin, Nε-t-Butyloxycarbonyl-L-lysyl-L-prolyl-L-valyl-glycin und Derivate. *Helv. Chim. Acta* **1961**, *44* (1), 159−169.
(58) Bergmann, M.; Zervas, L. Über ein allgemeines Verfahren der Peptid-Synthese. *Ber. Dtsch. Chem. Ges. B* **1932**, *65* (7), 1192−1201.
(59) Iatrou, H.; Dimas, K.; Gkikas, M.; Tsimblouli, C.; Sofianopoulou, S. Polymersomes from Polypeptide Containing Triblock Co- and Terpolymers for Drug Delivery against Pancreatic Cancer: Asymmetry of the External Hydrophilic Blocks. *Macromol. Biosci.* **2014**, *14* (9), 1222−1238.
(60) Nordmeier, E.; Lechner, M. D. Simultaneous Frequency-Integrated and Incoherent-Elastic Light Scattering: Description of a New Photon-Correlation Spectrometer. *Polym. J.* **1989**, *21* (8), 623−632.
(61) Konishi, T.; Yoshizaki, T.; Yamakawa, H. On the "Universal Constants" ρ and Φ. of flexible polymers. *Macromolecules* **1991**, *24* (20), 5614−5622.
(62) Qin, A.; Tian, M.; Ramireddy, C.; Webber, S. E.; Munk, P.; Tuzar, Z. Polystyrene-poly(methacrylic acid) block copolymer micelles. *Macromolecules* **1994**, *27* (1), 120−127.
(63) Yamakawa, H. *Modern Theory of Polymer Solutions*; Harper and Row: New York, 1971.
(64) Hayashi, T.; Kanai, H.; Yodoya, S.; Oka, M.; Hayashi, T. Biodegradation of random co-polypeptide hydrogels consisting of N-hydroxypropyl L-glutamine as one component. *Eur. Polym. J.* **2002**, *38* (1), 139−146.
(65) Thornton, P. D.; Billah, S. M. R.; Cameron, N. R. Enzyme-Degradable Self-Assembled Hydrogels From Polyalanine-Modified Poly(ethylene glycol) Star Polymers. *Macromol. Rapid Commun.* **2013**, *34* (3), 257−262.
(66) Jeong, Y.; Joo, M. K.; Bahk, K. H.; Choi, Y. Y.; Kim, H.-T.; Kim, W.-K.; Jeong Lee, H.; Sohn, Y. S.; Jeong, B. Enzymatically degradable temperature-sensitive polypeptide as a new in-situ gelling biomaterial. *J. Controlled Release* **2009**, *137* (1), 25−30.
(67) Matsui, M.; Fowler, J. H.; Walling, L. L. Leucine aminopeptidases: diversity in structure and function. *Biol. Chem.* **2006**, *387* (12), 1535−1544.
(68) Nelson, D. L. *Lehninger Principles of Biochemistry*, 4th ed.; W.H. Freeman: New York, 2005.
(69) Bantan-Polak, T.; Kassai, M.; Grant, K. B. A comparison of fluorescamine and naphthalene-2,3-dicarboxaldehyde fluorogenic reagents for microplate-based detection of amino acids. *Anal. Biochem.* **2001**, *297* (2), 128−136.
(70) Kim, K. T.; Zhu, J.; Meeuwissen, S. A.; Cornelissen, J. J. L. M.; Pochan, D. J.; Nolte, R. J. M.; van Hest, J. C. M. Polymersome Stomatocytes: Controlled Shape Transformation in Polymer Vesicles. *J. Am. Chem. Soc.* **2010**, *132* (36), 12522−12524.
(71) Wilson, D. A.; Nolte, R. J. M.; van Hest, J. C. M. Entrapment of Metal Nanoparticles in Polymer Stomatocytes. *J. Am. Chem. Soc.* **2012**, *134* (24), 9894−9897.
(72) Salva, R.; Le Meins, J.-F.; Sandre, O.; Brulet, A.; Schmutz, M.; Guenoun, P.; Lecommandoux, S. Polymersome Shape Transformation at the Nanoscale. *ACS Nano* **2013**, *7* (10), 9298−9311.
(73) Abdelmohsen, L. K. E. A.; Nijemeisland, M.; Pawar, G. M.; Janssen, G.-J. A.; Nolte, R. J. M.; van Hest, J. C. M.; Wilson, D. A. Dynamic Loading and Unloading of Proteins in Polymeric Stomatocytes: Formation of an Enzyme-Loaded Supramolecular Nanomotor. *ACS Nano* **2016**, *10* (2), 2652−2660.
(74) Tu, Y.; Peng, F.; Sui, X.; Men, Y.; White, P. B.; van Hest, J. C. M.; Wilson, D. A. Self-propelled supramolecular nanomotors with temperature-responsive speed regulation. *Nat. Chem.* **2017**, *9* (5), 480−486.
(75) Adawy, A.; Amghouz, Z.; van Hest, J. C. M.; Wilson, D. A. Sub-Micron Polymeric Stomatocytes as Promising Templates for Confined Crystallization and Diffraction Experiments. *Small* **2017**, *13* (28), 1−8.
(76) Pijpers, I. A. B.; Abdelmohsen, L. K. E. A.; Williams, D. S.; van Hest, J. C. M. Morphology Under Control: Engineering Biodegradable Stomatocytes. *ACS Macro Lett.* **2017**, *6* (11), 1217−1222.
(77) Shao, J.; Pijpers, I. A. B.; Cao, S.; Williams, D. S.; Yan, X.; Li, J.; Abdelmohsen, L. K. E. A.; van Hest, J. C. M. Biomorphic Engineering

DOI: 10.1021/acs.biomac.9b01331
Biomacromolecules XXXX, XXX, XXX−XXX

of Multifunctional Polylactide Stomatocytes toward Therapeutic Nano-Red Blood Cells. *Adv. Sci.* **2019**, *6* (5), 1801678.
(78) Tu, Y.; Peng, F.; Heuvelmans, J. M.; Liu, S.; Nolte, R. J. M.; Wilson, D. A. Motion Control of Polymeric Nanomotors Based on Host-Guest Interactions. *Angew. Chem., Int. Ed.* **2019**, *58* (26), 8687−8691.
(79) Kwoh, D. Y.; Coffin, C. C.; Lollo, C. P.; Jovenal, J.; Banaszczyk, M. G.; Mullen, P.; Phillips, A.; Amini, A.; Fabrycki, J.; Bartholomew, R. M.; Brostoff, S. W.; Carlo, D. J. Stabilization of poly-L-lysine/DNA polyplexes for in vivo gene delivery to the liver. *Biochim. Biophys. Acta, Gene Struct. Expression* **1999**, *1444* (2), 171−190.
(80) Yao, J. C.; Lombard-Bohas, C.; Baudin, E.; Kvols, L. K.; Rougier, P.; Ruszniewski, P.; Hoosen, S.; St. Peter, J.; Haas, T.; Lebwohl, D.; Van Cutsem, E.; Kulke, M. H.; Hobday, T. J.; O'Dorisio, T. M.; Shah, M. H.; Cadiot, G.; Luppi, G.; Posey, J. A.; Wiedenmann, B. Daily oral everolimus activity in patients with metastatic pancreatic neuroendocrine tumors after failure of cytotoxic chemotherapy: a phase II trial. *J. Clin. Oncol.* **2010**, *28* (1), 69−76.
(81) Jensen, R. T.; Cadiot, G.; Brandi, M. L.; de Herder, W. W.; Kaltsas, G.; Komminoth, P.; Scoazec, J.-Y.; Salazar, R.; Sauvanet, A.; Kianmanesh, R. ENETS Consensus Guidelines for the Management of Patients with Digestive Neuroendocrine Neoplasms: Functional Pancreatic Endocrine Tumor Syndromes. *Neuroendocrinology* **2012**, *95* (2), 98−119.
(82) Sabatini, D. M. mTOR and cancer: insights into a complex relationship. *Nat. Rev. Cancer* **2006**, *6* (9), 729−734.
(83) Zoncu, R.; Efeyan, A.; Sabatini, D. M. mTOR: from growth signal integration to cancer, diabetes and ageing. *Nat. Rev. Mol. Cell Biol.* **2011**, *12* (1), 21−35.
(84) Lamberti, G.; Brighi, N.; Maggio, I.; Manuzzi, L.; Peterle, C.; Ambrosini, V.; Ricci, C.; Casadei, R.; Campana, D. The role of mTOR in neuroendocrine tumors: future cornerstone of awinning strategy? *Int. J. Mol. Sci.* **2018**, *19* (3), 747.
(85) Houdaihed, L.; Evans, J. C.; Allen, C. Codelivery of Paclitaxel and Everolimus at the Optimal Synergistic Ratio: A Promising Solution for the Treatment of Breast Cancer. *Mol. Pharmaceutics* **2018**, *15* (9), 3672−3681.

DOI: 10.1021/acs.biomac.9b01331
Biomacromolecules XXXX, XXX, XXX−XXX